Molecular Therapy
Nucleic Acids
Original Article

Integrating IL-12 mRNA nanotechnology with SBRT eliminates T cell exhaustion in preclinical models of pancreatic cancer

Angela L. Hughson,[1,12] Gary Hannon,[1,12] Noah A. Salama,[2] Tara G. Vrooman,[2] Caroline A. Stockwell,[3] Bradley N. Mills,[1] Jesse Garrett-Larsen,[1] Haoming Qiu,[4] Roula Katerji,[5] Lauren Benoodt,[6] Carl J. Johnston,[7] Joseph D. Murphy,[2] Emma Kruger,[2] Jian Ye,[1] Nicholas W. Gavras,[1] David C. Keeley,[1] Shuyang S. Qin,[2] Maggie L. Lesch,[2] Jason B. Muhitch,[8] Tanzy M.T. Love,[9] Laura M. Calvi,[10] Edith M. Lord,[2] Nadia Luheshi,[11] Jim Elyes,[11] David C. Linehan,[1] and Scott A. Gerber[1,2,3]

[1]Department of Surgery, University of Rochester Medical Center, Rochester, NY, USA; [2]Department of Microbiology and Immunology, University of Rochester Medical Center, Rochester, NY, USA; [3]Department of Biomedical Engineering, University of Rochester, Rochester, NY, USA; [4]Department of Radiation Oncology, University of Rochester Medical Center, Rochester, NY, USA; [5]Department of Pathology and Laboratory Medicine, University of Rochester Medical Center, Rochester, NY, USA; [6]University of Rochester Genomics Center, University of Rochester Medical Center, Rochester, NY, USA; [7]Department of Pediatrics, University of Rochester Medical Center, Rochester, NY, USA; [8]Department of Immunology, Roswell Park Comprehensive Cancer Center, Buffalo, NY, USA; [9]Department of Biostatistics and Computational Biology, University of Rochester Medical Center, Rochester, NY, USA; [10]Department of Medicine, University of Rochester Medical Center, Rochester, NY, USA; [11]Oncology R&D, AstraZeneca, The Discovery Centre, Cambridge Biomedical Campus, Cambridge, UK

Pronounced T cell exhaustion characterizes immunosuppressive tumors, with the tumor microenvironment (TME) employing multiple mechanisms to elicit this suppression. Traditional immunotherapies, such as immune checkpoint blockade, often fail due to their focus primarily on T cells. To overcome this, we utilized a proinflammatory cytokine, interleukin (IL)-12, that re-wires the immunosuppressive TME by inducing T cell effector function while also repolarizing immunosuppressive myeloid cells. Due to toxicities observed with systemic administration of this cytokine, we utilized lipid nanoparticles encapsulating mRNA encoding IL-12 for intratumoral injection. This strategy has been proven safe and tolerable in early clinical trials for solid malignancies. We report an unprecedented loss of exhausted T cells and the emergence of an activated phenotype in murine pancreatic ductal adenocarcinoma (PDAC) treated with stereotactic body radiation therapy (SBRT) and IL-12mRNA. Our mechanistic findings reveal that each treatment modality contributes to the T cell response differently, with SBRT expanding the T cell receptor repertoire and IL-12mRNA promoting robust T cell proliferation and effector status. This distinctive T cell signature mediated marked growth reductions and long-term survival in local and metastatic PDAC models. This is the first study of its kind combining SBRT with IL-12mRNA and provides a promising new approach for treating this aggressive malignancy.

INTRODUCTION

T cell exhaustion is a state of dysfunction where T cells gradually lose effector function including impaired proliferation, decreased cytokine production, and an inability to kill tumor cells.[1] In addition to repeated antigen exposure, the immunosuppressive tumor microenvironment (TME) exacerbates T cell exhaustion through multiple mechanisms, including the secretion of suppressive cytokines, upregulation of inhibitory receptors on both tumor and effector immune cells, and the establishment of metabolic competition, favoring tumor cells over T cells for essential nutrients.[2] Treatments aimed at reversing T cell exhaustion, such as immune checkpoint blockade (ICB), often fall short due to their predominant focus on intratumoral T cells, neglecting to address the abundant immunosuppressive mechanisms exerted by the TME.[3] Therefore, developing novel therapeutic strategies that simultaneously target the reversal of T cell exhaustion *and* the immunosuppressive TME are required.

Interleukin (IL)-12, a potent proinflammatory cytokine with broad immunomodulatory effects, has been investigated as a therapeutic agent to enhance T cell effector function and reverse immunosuppressive myeloid cell polarization in advanced solid tumors.[4] Unfortunately, systemic administration of this cytokine resulted in dose-limiting toxicities and produced only modest outcomes in patients.[5,6] To overcome these initial clinical hurdles, our laboratory investigated strategies to deliver IL-12 directly to the tumor and optimize its antitumor potential. We discovered that radiotherapy, acting as an *in situ* vaccine, could enhance IL-12 potency in multiple tumor models. Our

Received 25 April 2024; accepted 26 September 2024;
https://doi.org/10.1016/j.omtn.2024.102350.

[12]Co-first authors

Correspondence: Scott A. Gerber, University of Rochester Medical Center, 601 Elmwood Avenue, Rochester, NY 14642, USA.
E-mail: scott_gerber@urmc.rochester.edu

previous work demonstrated that local delivery of recombinant IL-12 protein encapsulated in microspheres combined with stereotactic body radiation therapy (SBRT) was particularly effective in pancreatic ductal adenocarcinoma (PDAC), an aggressive malignancy refractory to most therapies.[7] Building on this, our current study introduces a next-generation approach where IL-12 is delivered intratumorally via mRNA encapsulated in a lipid nanoparticle. We chose this particular platform as intratumoral delivery of the human equivalent of this IL-12mRNA has already been proven safe and tolerable in phase I clinical trials across multiple cancer patients, including PDAC (NCT03946800).[8]

In this study, we utilized mRNA delivery of IL-12 that consists of a transcript encoding both p35 and p40 subunits of the cytokine fused with a polypeptide linker and incorporates an miR122 binding domain to limit off-site translation in the liver.[9] When administered intratumorally, IL-12mRNA directs cells within the tumor microenvironment (TME) to produce IL-12 locally, thereby concentrating the therapeutic payload to the tumor. As expected, the local production of IL-12 shifted the TME toward immunostimulation; however, this particular technology outperformed our previous work by also inducing a dramatic transformation in the T cell landscape, effectively mitigating the exhaustive phenotype. Consequently, the reinvigorated intratumoral T cells exhibited heightened activation and robust proliferation, features typically absent within the immunosuppressive PDAC TME. Mechanistic studies revealed that the stimulation of T cells was mainly attributed to the effects of IL-12mRNA. Optimal efficacy of IL-12mRNA therapy was achieved only when combined with SBRT, however, which acted to expand the T cell receptor repertoire, enabling T cells to respond against a broader spectrum of tumor antigens. The synergistic effects of SBRT and IL-12mRNA resulted in cures and long-term survival in multiple aggressive models of PDAC.

Our study describes the first use of SBRT in combination with IL-12mRNA in PDAC. Even more significant is that this combination achieved unprecedented reinvigoration of exhausted T cells, representing a breakthrough currently unattainable through checkpoint blockade in this specific cancer.[10] Building on the established safety, tolerability, and feasibility of intratumoral delivery of IL-12mRNA in early trials,[8] coupled with the standard practice of treating localized PDAC with SBRT,[11,12] our study presents rationale for the investigation of this innovative combination treatment in combating this aggressive malignancy.

RESULTS

Local delivery of SBRT and IL-12mRNA therapy eliminates primary disease and promotes durable, systemic antitumor immunity

We developed a model where both SBRT and immunotherapy were delivered locally to the primary pancreatic tumor (Figure 1A). Mice were injected orthotopically with the luciferase-expressing KP2 cell line and established tumors were treated with a clinically relevant dose and schedule of SBRT consisting of 6 Gy/d for 4 consecutive days. One day following the final fraction of SBRT, an intratumoral injection of IL-12mRNA or scrambled control mRNA (scr-mRNA; non-translating) was administered and tumor burden was monitored by luciferase-detecting in vivo imaging systems (IVIS) along with survival. This regimen resulted in four treatment groups: (1) No SBRT + scr-mRNA (hereafter referred to as "Untreated"), (2) SBRT + scr-mRNA ("SBRT"), (3) No SBRT + IL-12mRNA ("IL-12mRNA"), and (4) SBRT + IL-12mRNA ("SBRT/IL-12mRNA"). SBRT/IL-12mRNA was superior to each monotherapy and resulted in a dramatic reduction of primary tumor burden (Figure 1B) including long-term survival (Figure 1C) past 300 days. Cured mice rested for 6 weeks following SBRT/IL-12mRNA treatment were able to reject a hepatic challenge of PDAC demonstrating long-term systemic immunity (Figure 1D). The aggressive KP2 cell line used in the experiments described above has driver mutations in *KRAS* and *TP53*; a phenotype that accounts for approximately 70% of human PDAC patients.[13] We tested whether SBRT/IL-12mRNA was effective in other variants of PDAC, including mutated *KRAS* only (KCKO cell line) and the highly aggressive and incurable spontaneous KPC (LSL-$Kras^{G12D}$; $Tp53^{L/L}$; P48-Cre) mouse model that develops tumors throughout the entire pancreas.[14] Similar to the KP2 model, SBRT/IL-12mRNA was highly efficacious against KCKO tumors (Figures S1A–S1C) and provided a significant survival advantage in homozygous KPC mice (Figure S1D).

To test the systemic effects of our therapy, we generated a clinically relevant metastatic model where localized therapy was administered to the primary tumor alone to determine whether distal effects could be achieved. Mice were injected with primary orthotopic pancreatic tumors as illustrated in Figure 1A and concurrently given a portal vein injection to recapitulate distal hepatic metastases; the most common site for PDAC dissemination (Figure 1E). Even though only the primary tumor received SBRT/IL-12mRNA treatment, significant distal effects to liver metastasis were observed that corresponded to long-term survival in 67% of mice (Figures 1F and 1G). Similar systemic antitumor immunity was also observed using the KCKO metastatic model (Figures S1E and S1F). Collectively, these data demonstrate that localized delivery of SBRT and IL-12mRNA eliminates primary PDAC tumors and promotes systemic immunity capable of controlling distal metastatic disease.

IL-12mRNA administered to the TME results in local concentrations of IL-12 protein

We quantified the concentration of IL-12 protein following intratumoral administration of IL-12mRNA and whether this cytokine was confined locally. As illustrated in Figure S2A, SBRT/IL-12mRNA results in the highest production of intratumoral IL-12 at 24 h, which returns to near baseline at 96 h. Similar concentrations and kinetics were detected in the pancreatic draining lymph node (dLN) (Figure S2B); however, near 20-fold lesser concentrations were measured in distal tissues such as the liver and non-draining lymph node (ndLN) at 24 h, and no IL-12 protein above controls was detected at 96 h (Figures S2C and S2D). Notably, blood levels of liver and kidney functional markers remained within normal physiological levels after treatment and, when elevations were detected

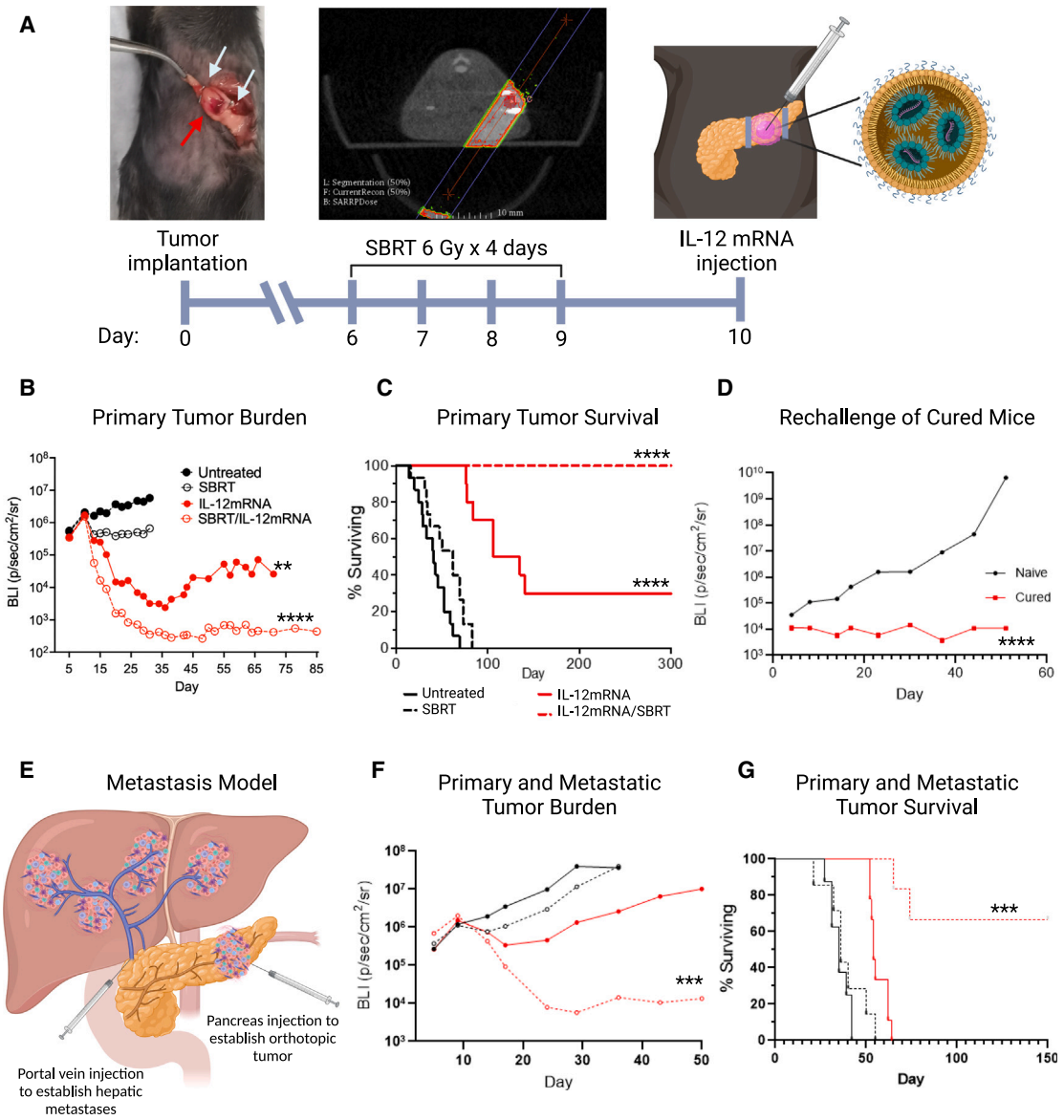

Figure 1. Combination treatment of SBRT + IL-12mRNA eliminates pancreatic tumors and promotes survival

(A) Illustration of PDAC mouse model where 2.5 × 10^4 KP2-luciferase-expressing tumor cells were injected orthotopically (red arrow) and flanked with titanium fiducial clips (white arrows) for SBRT targeting. The tumors were treated with or without SBRT (6 Gy/d over 4 consecutive days) followed by an intratumoral injection of IL-12mRNA or control scr-mRNA 1 day after the final fraction of radiation. (B) Tumor burden for primary disease was assessed by weekly BLI measurements for each treatment. (C) Survival was tracked out to 300 days post tumor injection. (D) BLI growth curve for systemic rechallenge of cured mice versus aged-matched naive mice (E) Illustration of the metastatic model developed to test the systemic effects SBRT/IL-12mRNA treatment: pancreas and hepatic portal vein were injected concurrently to establish primary (pancreas) and metastatic (liver) tumors. (F) BLI growth curve for each treatment for the metastatic PDAC model. (G) Survival curve for the metastatic model was tracked out to 150 days. n = 15/group from three independent experiments in (B) and (C). n = 5 for cured mice and n = 9 aged-matched naive mice in (D). n = 6–8 in (F) and (G). For BLI growth curves, mean values for each time point are presented for each treatment group. $^{**}p < 0.01$; $^{***}p < 0.001$; $^{****}p < 0.0001$.

(albeit still within normal ranges; such as alanine transaminase), these resolved within 2 weeks of IL-12mRNA treatment (Figure S2E).[15]

The production of IL-12 protein suggests that IL-12mRNA was being taken up and translated to protein by cells in the TME. We performed *in vitro* assays to identify which cells were responsible for this production. Cell subsets commonly found in the PDAC TME (tumor cells, fibroblasts, lymphocytes, and macrophages) were cultured with either IL-12mRNA or scr-mRNA sequence and qPCR was used to determine mRNA uptake by detecting a unique RNA sequence located in the IL-12mRNA. All cells analyzed were able to take up abundant IL-12mRNA when compared with scr-mRNA controls

(Figure S2F); however, only fibroblasts and especially tumor cells and macrophages produced IL-12 protein following uptake (Figure S2G). These data demonstrate that intratumoral administration of IL-12mRNA results in elevated local concentrations of IL-12 protein in the TME likely produced by tumor and host stromal/myeloid cells.

Analysis of the TME following SBRT/IL-12mRNA

The PDAC TME is highly immunosuppressive and represents a major barrier to treatment efficacy. We assessed whether SBRT/IL-12mRNA therapy modulated the TME. Histological assessment of the TME by a blinded board-certified pathologist revealed a poorly differentiated carcinoma surrounded by desmoplastic stroma and mild inflammatory infiltrate in all groups at 72-h post scr-mRNA/IL-12mRNA treatment (Figure S3A). Of note were minor increases of fibrosis in the SBRT-only group, no definitive treatment response in the IL-12mRNA-only group, but appreciable treatment response in the SBRT/IL-12mRNA group defined as fibrosis, foci of necrosis, hyalinization, and mixed inflammatory infiltrate. Following histological evaluation, we focused on examining the cellular composition within the tumor to determine how SBRT/IL-12mRNA therapy influences the immune landscape. Local delivery of SBRT/IL-12mRNA did not alter the percentage of intratumoral CD45+ immune cells as assessed by flow cytometry (gating scheme defined in Figure S4) at 24- and 72-h post IL-12mRNA treatment (Figure S3B). A flow cytometric immune subset analysis revealed a variety of intratumoral immune cells with macrophages occupying the largest density (Figure S3C). Notably, the only significant changes we observed were a reduction of radiosensitive CD4 and B lymphocytes at 24 h (Figures S3D and S3E). At 72 h, most of these changes returned to control levels. Collectively, only SBRT/IL-12mRNA demonstrated notable pathological changes in the TME, however the tumor immune cell infiltrate was largely similar between all groups.

Transcriptomic analysis of the TME following SBRT/IL-12mRNA

Since no appreciable differences were seen in the quantity of intratumoral immune cells following therapy (Figures S3B and S3C), we hypothesized SBRT/IL-12mRNA may enhance the quality of these cells. Single-cell RNA sequencing (scRNA-seq) was utilized to assess transcriptomic differences induced by SBRT/IL-12mRNA. Following quality control and filtering steps, over 11,000 intratumoral cells from each treatment group were sequenced as detailed in the materials and methods. Unsupervised clustering of all cells identified 29 distinct clusters, which were further annotated into distinct cell subsets based on canonical markers and assembled into four larger groups namely tumor/stromal cells, myeloid cells, B cells, and T/NK cells (Figure 2A). Individual uniform manifold approximation and projection (UMAPs) plots were generated for each treatment condition (Figure 2B) and the relative position of four major cellular groups was assessed between each treatment. The myeloid and T/NK cell groups demonstrated appreciable positional movement through the UMAP as conditions progressed from untreated to SBRT/IL-12mRNA suggesting transcriptomic differences attributed to therapy. Therefore, we focused our analysis on these two intratumoral cell subsets.

SBRT/IL12mRNA repolarizes immunosuppressive myeloid cells to an immunostimulatory phenotype

The immunostimulatory/suppressive phenotype of intratumoral myeloid cells was assessed by single-cell RNA sequencing (scRNA-seq) following initial observations of considerable changes following treatment (Figure 2B; see red and black regions denoting transcriptomic changes in the myeloid cell population). Myeloid populations were subclustered (Figure S5A), and based on canonical markers, resulted in predominate populations of neutrophils and dendritic cells (DCs), macrophages and monocytes, and neutrophils (Figure S5B). SBRT/IL12mRNA resulted in heightened expression of many immunostimulatory genes when either all myeloid cells or each individual subset were examined against untreated and SBRT-only groups (Figure S6). These data illustrate the repolarization of intratumoral myeloid cell populations following SBRT/IL-12mRNA therapy.

As the most abundant immune population in the tumor (Figure S3C), macrophages were explored further for changes across the four treatment groups (Figure 3). Transcriptomic analysis identified two distinct macrophage populations with alternatively activated (immunosuppressive) and classically activated (immunostimulatory) phenotypes (Figure 3A), as defined by immuno-suppressive/stimulatory canonical markers (Figure 3B). The vast majority of macrophages in untreated tumors exhibited an alternatively activated phenotype, which remained largely unchanged with SBRT treatment. However, both IL-12mRNA and SBRT/IL-12mRNA treatments induced a marked repolarization toward a classically activated phenotype (Figures 3C and 3D). To corroborate these findings, flow cytometry was performed on day 13 tumors (3 days post IL-12mRNA/scr-mRNA treatment) to assess macrophage phenotype. Surface and intracellular markers associated with either immunosuppression (arginase-1, CD163, CD206, PDL1) or immunostimulation (interferon [IFN]γ, major histocompatibility complex [MHC]II, MHCI) were used for characterization. Subsequent principal-component analysis of these markers revealed that macrophages from IL-12mRNA and SBRT/IL-12mRNA clustered together, indicating similar effects on these cells, whereas macrophages from SBRT and untreated tumors were grouped closely, reflecting similar profiles (Figure 3E). Utilizing CD206 and IFNγ as representative markers, IL-12mRNA and SBRT/IL12mRNA treatments led to a reduction in immunosuppressive macrophages (CD206+) and a corresponding increase in macrophages with a more immunostimulatory phenotype (IFNγ+) (Figures 3F and 3G). Overall, SBRT/IL-12mRNA repolarizes immunosuppressive macrophages in tumors, which is largely driven by IL-12mRNA.

T cells undergo transcriptomic changes following treatment and are essential to mediate SBRT/IL-12mRNA efficacy

Cells within the T/NK cell green quadrilateral demonstrated the most visible UMAP changes (Figure 2B; see red and black regions denoting transcriptomic changes in the T/NK cell population). These data emphasize the greatest impact of SBRT/IL-12mRNA on this immune subset and complemented subsequent depletion studies, which also identified T cells as the chief cells responsible for treatment efficacy

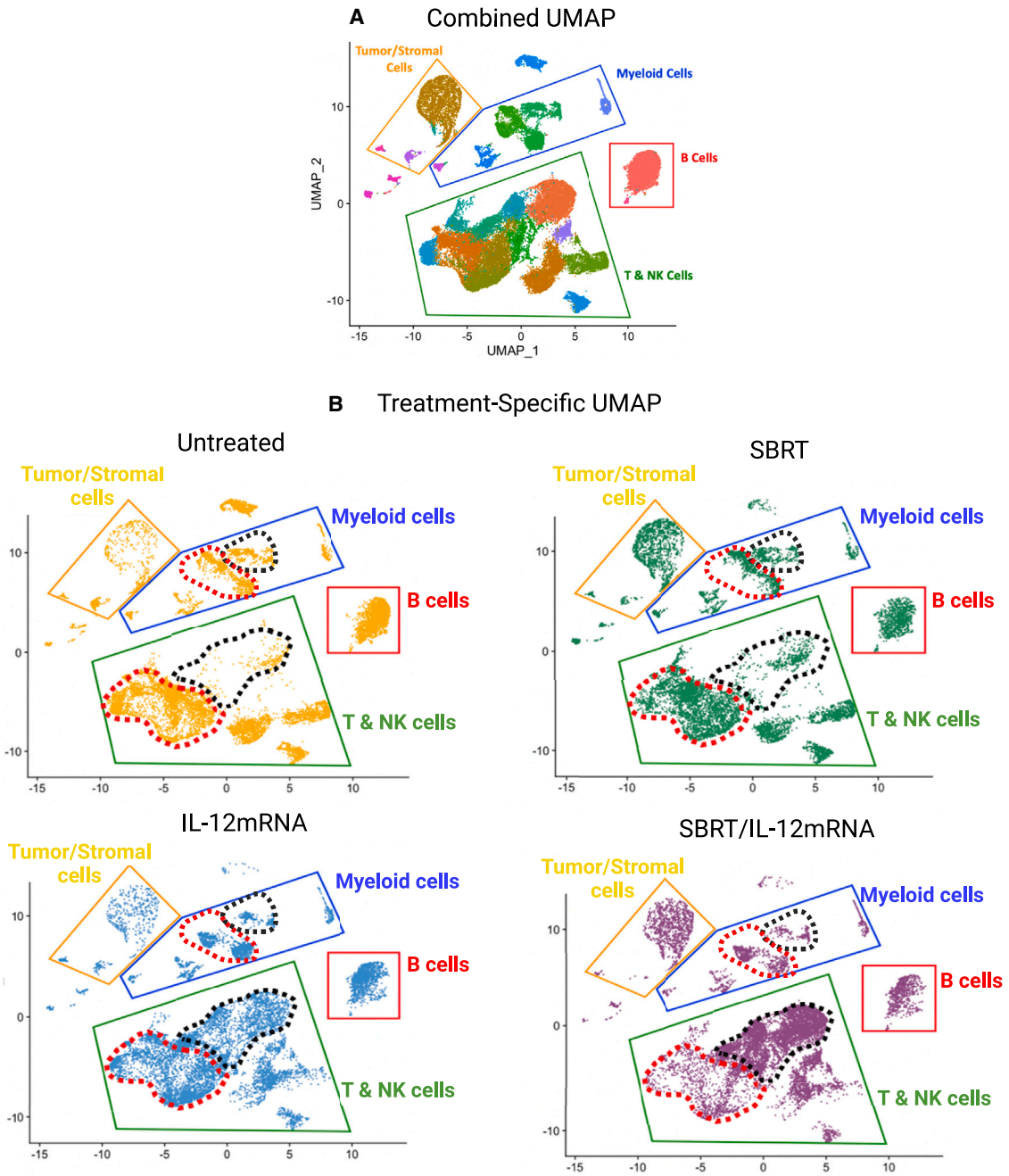

Figure 2. T cells undergo distinct transcriptomic changes following SBRT/IL-12mRNA treatment

(A) Unsupervised clustering of intratumoral cells following scRNA-seq could identify four distinct cell subsets: Tumor/Stromal cells, Myeloid cells, B cells and T/NK cells. (B) Separating this clustering to treatment-specific UMAPs could identify significant transcriptomic changes to T cells and myeloid, in particular, following SBRT/IL-12mRNA treatment (see red and black highlighted regions). See materials and methods for further details.

(Figures S7A–S7C). Depletion of NK cells, by contrast, had no effect on treatment outcome (Figure S7D). Given these results, we directed our analysis on subclustered T cells based on expression of CD4 and CD8 along with coexpression of CD3ε and T cell receptor (TCR)α/β gene signatures. Utilizing canonical markers, differentially expressed genes (DEGs) (Figures S8A and S8B), and curated gene signatures, we identified five distinct CD4 T cell subsets (Naive, T-regulatory, Exhausted, Intermediate, Activated/Cycling) and four CD8 T cell

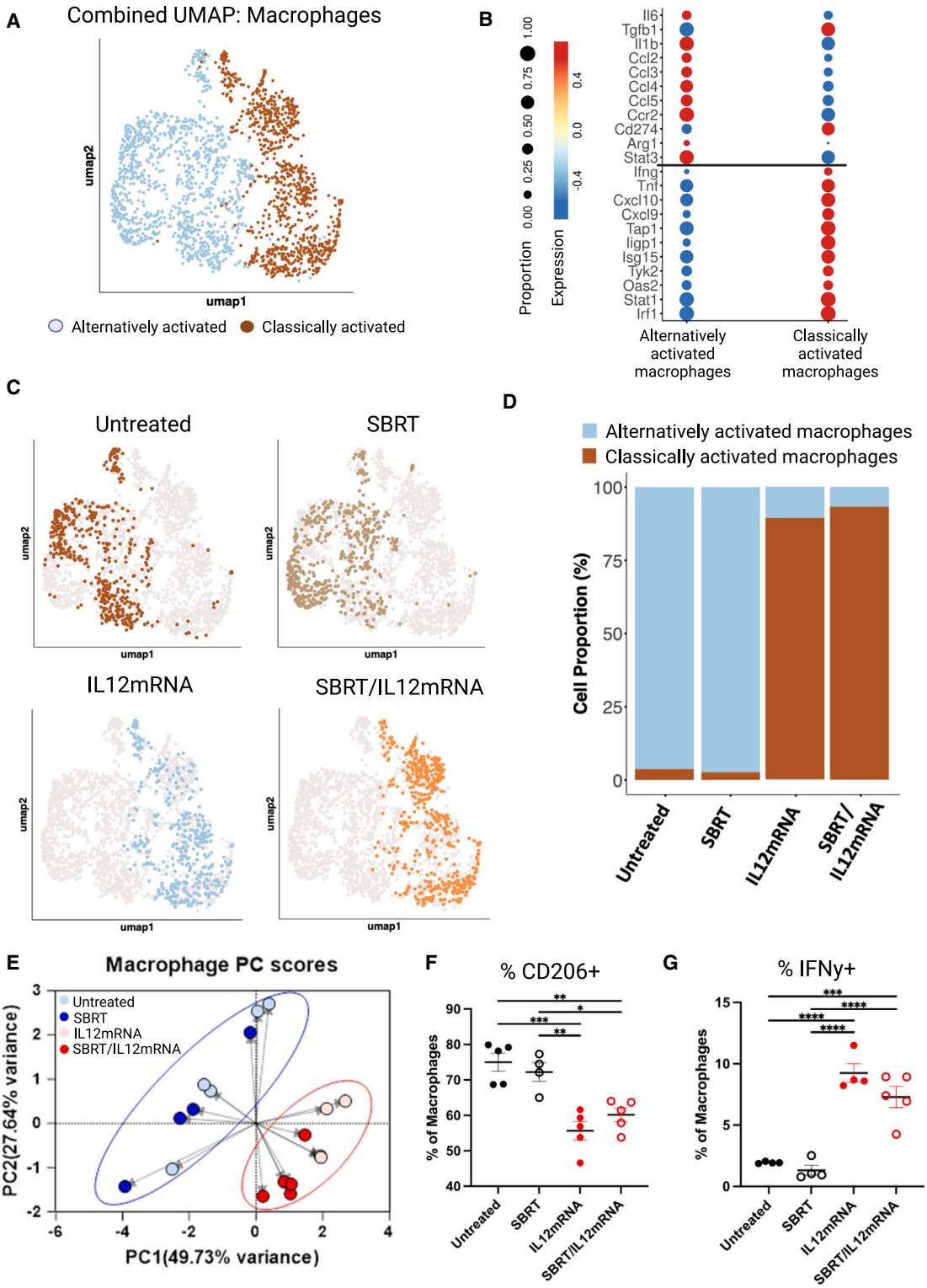

Figure 3. Modulations to macrophages after SBRT/IL12mRNA treatment

(A) Combined UMAP for all macrophages across the four treatment groups. (B) Expression and relative proportion levels of key genes to classify classically and alternatively activated macrophages. (C) UMAP of macrophage populations for each treatment group. (D) Relative proportions of classically and alternatively activated macrophages for

(legend continued on next page)

subsets (Naive, Exhausted, Intermediate, Activated/Cycling). Naive and T-regulatory (CD4) subsets encompassed a relatively small percentage of total T cells. The much larger population of Exhausted T cells exhibited abundant expression of the hallmark *TOX, LAG3, HAVCR2, PDCD1,* and *RGS16* genes (Figures S9A and S9B). Interestingly, the Activated/Cycling population predominately expressed genes associated with cell division (*TOP2A, MKI67, RAD51, PCNA,* etc.), with only moderate expression of classical effector genes such as *IFNG GZMB, PRF1, TBX21*, etc. This is in contrast to the Intermediate subset, which had a far lesser proliferative signature, but heightened expression of effector genes (Figures S9A and S9B) Collectively, T cells mediate SBRT/IL-12mRNA efficacy for which we identified distinct larger subpopulations such as Exhausted, Intermediate, and Activated/Cycling that underwent profound transcriptomic changes following treatment.

SBRT/IL-12mRNA remodels T cell subsets toward an effector/activated phenotype

Individual UMAPs were generated for each treatment condition to parse out how each therapy was modulating T cell subsets. The vast majority of CD4 (95%) and CD8 (88%) T cells in untreated tumors exhibited transcriptomic signatures of Exhaustion (red population), Regulatory (CD4; blue population), or Naive (purple population) (Figures 4A and 4B, respectively) T cells. These results are in accordance with clinical PDAC data where most intratumoral T cells are dysfunctional and have an impaired ability to respond adequately against the tumor.[16] Although each monotherapy reduced the Naive and Exhausted populations and increased the Intermediate subsets, SBRT/IL-12mRNA resulted in the noted disappearance of Exhausted/Naive/Regulatory T cells and a significant expansion of the Activated/Cycling and Intermediate CD4 and CD8 T cell populations (Figures 4C–4E). Additionally, while IL-12mRNA alone led to an expansion of activated/cycling CD4 and CD8 T cells, these cells still maintained significantly higher expression of immunosuppressive transcripts (*TOX, HAVCR2, RGS16, LAG3, PDCD1, CTLA4*) when directly compared to the activated/cycling cells in the SBRT/IL-12mRNA treated group (Figures S10A and S10B).

Further analysis of the Exhausted CD4 T cell subpopulation by coexpression feature plots revealed the majority of *LAG3*-expressing cells (81%) did not express the proliferative marker *MKI67* in untreated tumors (Figure 4F). This is in contrast to SBRT/IL-12mRNA tumors where not only was there a marked reduction of *LAG3*-expressing T cells, but the proliferative signature shifted toward the Activated/Cycling population. Similar data were observed in CD8 T cells (Figure S10C).

We next examined the effector markers IFNγ and perforin (*PRF1*) to investigate whether SBRT/IL-12mRNA modulates the cytotoxicity profile of CD8 T cells. Treatment results in a complete conversion (96% of CD8) toward cells that either express IFNγ (32%) or both IFNγ and perforin (63%), suggestive of cytotoxic effector cells (Figure 4G).

Intratumoral T cells can transition between different functional states (e.g., exhausted, activated, etc.), based on the type of therapy. We performed unsupervised Monocle 3 pseudotime inference to assess how SBRT/IL-12mRNA modulates T cell trajectories. Black circles indicated branch nodes, where cells can travel to one of several outcomes, whereas white circles denote a potential terminal outcome of the cell trajectory. CD4 T cell pseudotime analysis using Naive T cells as the root population identified several trajectories depending on condition: T-regulatory cells (outcome 1), Exhausted T cells (outcome 2, 3), and the Intermediate T cell population (outcome 4, 5) (Figure 4H). Importantly, the CD4 Exhausted and Intermediate T cells were neighboring clusters connected by branchpoints along the pseudotime trajectories suggesting a possible transition between these two states. The Activated/Cycling CD4+ T cell population did not have terminal outcome nodes and was only connected to the Intermediate cluster suggesting that Activated/Cycling cells could give rise to the Intermediate population or that only the Intermediate population could enter the Activated/Cycling state. Similar results were observed in the CD8 T cell trajectory analysis where terminal outcome nodes only existed in the Exhausted and Intermediate subsets, but not the Activated/Cycling population (Figure 4I). Similar to CD4 T cells, a link also existed between the CD8 Intermediate population and the Activated/Cycling cells, but not between the Exhausted and Activated/Cycling populations.

Collectively, these data demonstrate that the Exhausted T cell subset observed almost exclusively in Untreated tumors is largely absent following SBRT/IL-12mRNA therapy and instead replaced with T cells exhibiting an activated/effector phenotype.

SBRT/IL-12mRNA induces intratumoral T cell proliferation

Cell cycle/proliferation was one of the strongest transcriptomic signatures observed in T cells following SBRT/IL-12mRNA. To further investigate this finding, we performed a Cell Cycle Score, which assesses expression of genes associated with different stages of cell cycle (G1; S-phase; G2/M), on both intratumoral CD4 (Figure 5A) and CD8 (Figure 5B) T cells. For both CD4 and CD8 T cells, the majority of Naive, Exhausted, and Intermediate cells exhibited a "G1" signature suggesting a phenotype of minimal proliferation. In contrast, the Activated/Cycling T cells formed a circular cluster with approximately one-half the cells in S-phase and the other half in G2/M. This strong proliferative signature shaped the UMAP essentially into dividing (cells in S-phase and G2/M) and non-dividing (G1) T cells.

each treatment group. (E) Principal-component analysis for macrophages based on protein expression of IFNγ, arginase-1, CD163, CD206, MHCII, MHCI, and PDL1 using flow cytometry on tumors from day 13 (3 days post IL-12mRNA/scr-mRNA injection). Ovals indicate groups of similar principal component scores. (F) Protein expression of CD206 on macrophages. (G) Protein expression of IFNγ on macrophages. $n = 5$ for (E), (F), and (G). Analyzed by one-way ANOVA followed by Tukey's test in (F) and (G). $^{*}p < 0.05$; $^{**}p < 0.01$; $^{***}p < 0.001$; $^{****}p < 0.0001$. Lines represent mean±standard error of the mean (SEM) in (F) and (G).

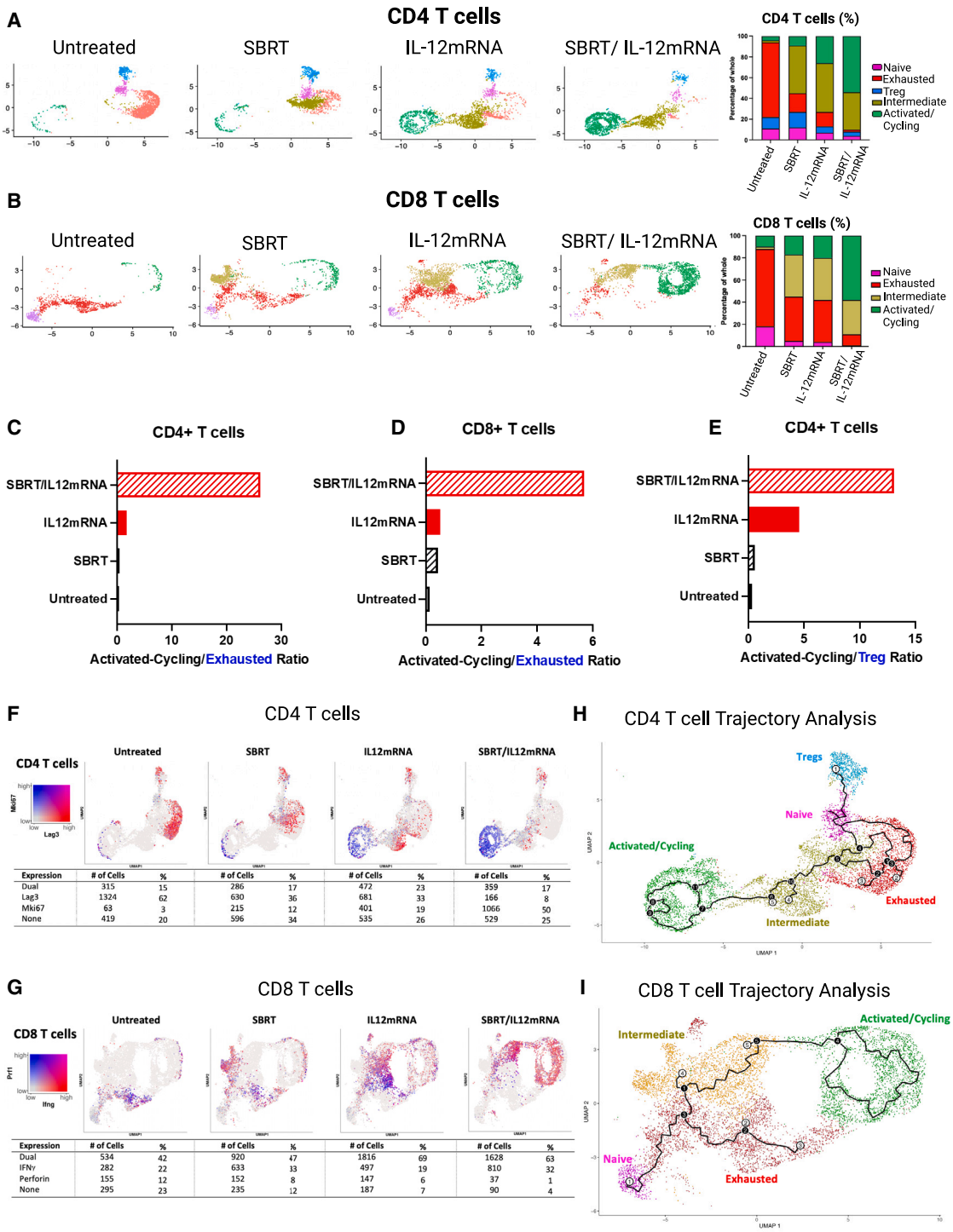

Figure 4. SBRT/IL-12mRNA treatment remodels the CD4 and CD8 T cell response in tumors

(A and B) Subclustered UMAPs and relative proportions of CD4 and CD8 T cell subpopulations following each treatment. (C and D) Ratios of activated/cycling to exhausted CD4 and CD8 T cells. (E) Ratios of activated/cycling to regulatory CD4 T cells. (F and G) Co-expression heatmaps for Mki67/Lag3 for CD4 T cells and Prf1/Ifng for CD8 T cells for each treatment. (H and I) Trajectory analysis for CD4 and CD8 T cells with Naive T cells utilized as the root population in each case. Black circles indicated branch nodes and white circles signify potential terminal outcomes along the trajectory. See materials and methods for further details.

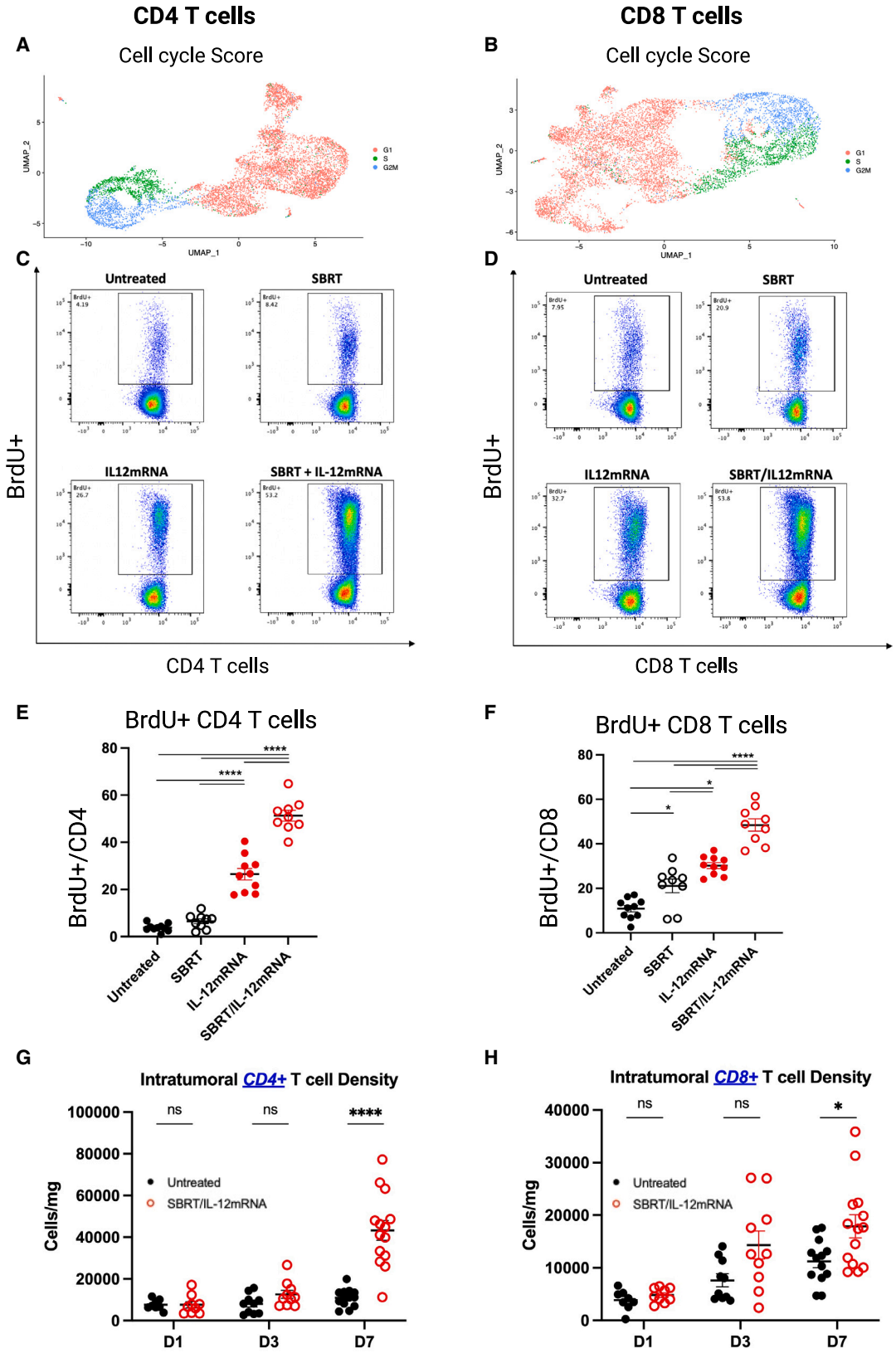

(legend on next page)

To validate these transcriptomic data, mice bearing KP2 tumors and treated as described in Figure 1A were administered BrdU 4 h before they were euthanized (3 days post IL-12mRNA/scr-mRNA treatment). BrdU incorporation signifying proliferating intratumoral T cells was assayed by flow cytometry. As illustrated in Figures 5C and 5D and quantified in Figures 5E and 5F, CD4 and CD8 T cells from untreated tumors had minimal BrdU incorporation, whereas T cells from tumors treated with SBRT/IL-12mRNA exhibited significant BrdU incorporation suggestive of robust proliferation. Approximately one-half of all intratumoral T cells were dividing, which strongly supports the transcriptomic results demonstrating increased expression of cell cycle/proliferation genes following SBRT/IL-12mRNA therapy.

Robust proliferation induced by SBRT/IL-12mRNA treatment resulted in an increased density of both intratumoral CD4 and CD8 T cells as determined by flow cytometry (Figures 5G and 5H, respectively). The elevated density of T cells was not immediate, but rather delayed as significant increases were not observed until 7 days after IL-12mRNA administration. Collectively, these data demonstrate that the combination of SBRT with IL-12mRNA results in vigorous cell division of intratumoral T cells, which in turn augments T cell density.

SBRT/IL-12mRNA results in a clonal TCR repertoire, which is largely a function of radiotherapy

Radiotherapy, through the release of antigen or provision of neoantigens, has been shown to remodel the TCR repertoire.[17,18] We investigated whether SBRT alone, or in combination with IL-12mRNA, modulates the repertoire by performing TCR sequencing on intratumoral T cells isolated from tumors 3 days after IL-12mRNA or scRNA administration (Figure 6A). We assessed the number of unique clonotypes of each treatment group using the well-established Chao1 Diversity/Clonality Score Index with downsampling to normalize input. Both CD4 and CD8 T cells from the SBRT and SBRT/IL-12mRNA groups exhibited a more clonal TCR repertoire when compared with untreated and IL-12mRNA (Figure 6B). This analysis considers the entire repertoire, therefore we focused on the top 1%, which likely represents the more dominant antitumor TCR clonotypes. Bubbleplots of these top clonotypes were presented from each treatment group in Figures 6C–6F. Each bubble/circle is indicative of one unique TCR clonotype, and the size of the circle represents how many copies (clones) make up that particular clonotype. Therefore, a larger size circle indicates clonal expansion of that particular clonotype, whereas smaller circles represent clonotypes that failed to expand. SBRT and SBRT/IL-12mRNA treatments resulted in more of the larger-sized circles suggesting that the top 1% of CD4 clonotypes underwent increased clonal expansion (Figure 6C; quantified in Figure 6D). In contrast, untreated and IL-12mRNA had a greater number of smaller circles (poorly expanded TCR clones). The increase in clonal expansion in the top 1% of the CD8 repertoire was more pronounced in the SBRT group with lesser expansion in the SBRT/IL-12mRNA group (yet higher than untreated and IL12mRNA) (Figure 6E; quantified in Figure 6F). Similar results were obtained when the entire downsampled population was examined (Figures S11A–S11D). Collectively, these data suggest that SBRT, rather than IL-12, is the driving factor that reshapes the TCR repertoire, which ultimately results in greater clonal expansion of the most dominant clones.

IFNγ mediates SBRT/IL-12mRNA efficacy

Many biological effects of IL-12 are mediated by IFNγ.[19] Additionally, IFNγ, along with IL-12, can skew CD4 T cells toward a Th1 type response that promotes antitumor immunity. This response is typically generated in the dLN, therefore we quantified the IFNγ concentration in the pancreatic dLN and observed a delayed induction of this key cytokine in both the IL-12mRNA alone and SBRT/IL-12mRNA groups (Figure S12A). Concordantly, a significant expression of the Th1-promoting transcription factor Tbet was observed in the dLN CD4 T cells in the SBRT/IL-12mRNA group (Figures S12B and S12C). These data indicate that local combination therapy can polarize immune cells toward an antitumor response in the distal dLN.

We shifted our focus to the tumor and quantified intratumoral IFNγ protein by Luminex in the four treatment groups at multiple time points following therapy. SBRT/IL-12mRNA resulted in elevated concentrations 24 h after therapy that were sustained for at least 96 h post therapy (Figure 7A). We assessed the production of IFNγ by intracellular flow cytometry of CD45+ cells (Figure S13A), and IL-12mRNA or SBRT/IL-12mRNA therapy augmented the density of these cells at both time points (Figure S13B). An immune subset analysis revealed that T cells, and to a lesser extent, NK and myeloid cells, were the predominant intratumoral populations generating IFNγ early; however, T cells dominated IFNγ production at later time points (Figures S13C and S13D). We focused our analysis on IFNγ+ T cells and showed that CD4 (∼30%) and CD8 (∼20%) had sustained IFNγ production over the 24- and 72-h timepoints in both the IL-12mRNA and SBRT/IL-12mRNA groups (Figure 7B).

We utilized scRNA-seq data to quantify the frequency and intensity (denoted by heatmap signatures) of each CD4 and CD8 T cell subset (e.g., Naive, Exhausted, etc.) that expressed an IFNγ transcriptomic signature. Figure 7C (farthest left) illustrates that the Intermediate population of both CD4 and CD8 T cells has the highest density of IFNγ expression when examining all treatment groups together.

Figure 5. SBRT/IL-12mRNA induces proliferation in tumor CD4 and CD8 T cells

(A and B) Cell cycle score for CD4 and CD8 T cells using genes associated with G1, S, and G2/M phases of cell cycle. (C and D) Representative flow graphs for BrdU staining in CD4 and CD8 T cells at 3 days post IL-12mRNA/scr-mRNA injection. (E and F) Quantification of BrdU+ CD4 and CD8 T cells. (G and H) CD4 and CD8 T cell tumor levels at day 1, day 3 and day 7 post IL-12mRNA/scr-mRNA injection. n = 10/group from two independent experiments in (C)–(H). One-way ANOVA followed by Tukey's test. Significance against untreated and between treatments are reported. $^{*}p < 0.05$; $^{****}p < 0.0001$. Lines represent mean ± SEM for (G) and (H).

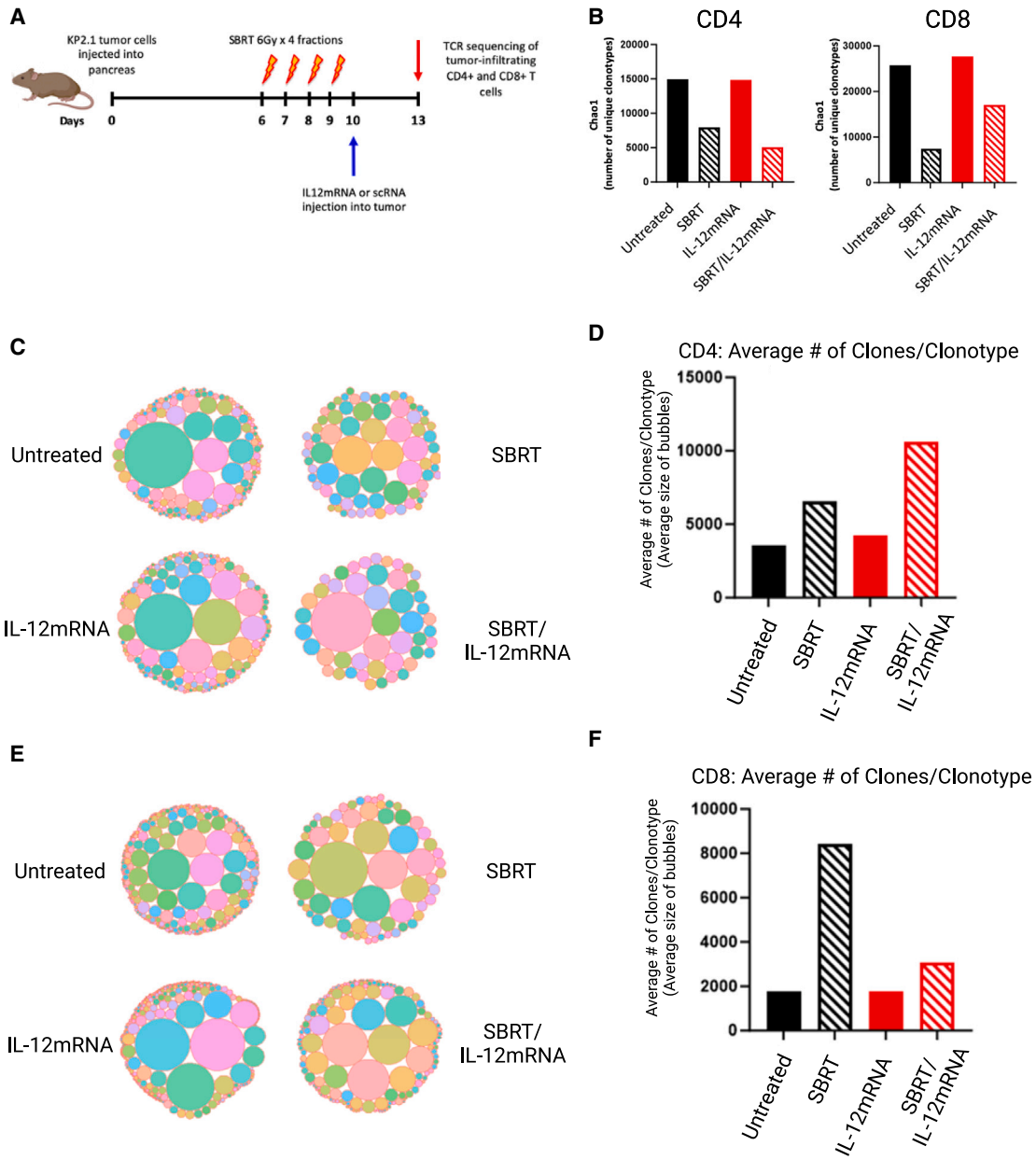

Figure 6. SBRT reshapes the TCR repertoire in tumors

(A) Illustration of experimental protocol for TCR sequencing analysis following SBRT/IL-12mRNA treatment: KP2 tumors are injected on day 0 and SBRT/IL-12mRNA treatment is given as described previously. Three days after IL-12mRNA/scr-mRNA injection, tumors are harvested, CD4 and CD8 T cells sorted, and their receptors sequenced. (B) Chao1 diversity index plot indicating the number of unique clonotypes for each treatment for both CD4 and CD8 T cells. (C) Bubble plots for the top clonotypes for each treatment group for CD4 T cells. (D) Bar charts depicting the average number of clonotypes for each treatment for CD4 T cells. (E) Bubble plots for the top clonotypes for each treatment group for CD8 T cells. (F) Bar charts depicting the average number of clonotypes for each treatment for CD8 T cells. See materials and methods for further details.

When examining each treatment group separately, a lesser IFNγ signature can be observed in the untreated and SBRT groups (66%), which increases after SBRT/IL-12mRNA treatment (95%) for both CD4 and CD8 T cells. This strong signature could also be appreciated when comparing relative expression levels across treatments, which was considerably higher in both IL-12mRNA and SBRT/IL-12mRNA groups (Figures S13E and S13F). Furthermore, the vast majority of all CD4 and CD8 T cells in the SBRT/IL-12mRNA group are expressing IFNγ with the Intermediate group possessing the higher expression when compared with the Activated/Cycling population.

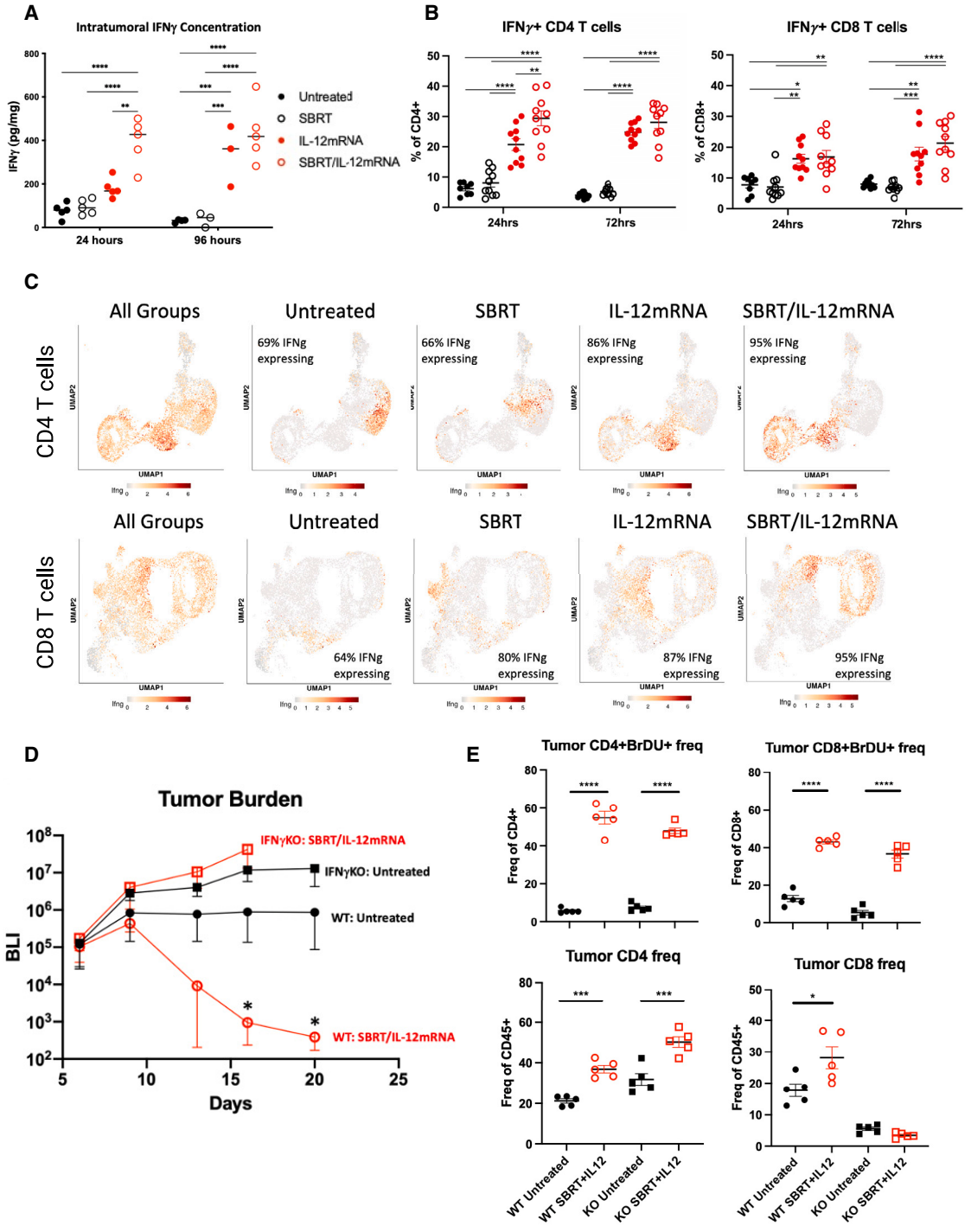

Figure 7. IFNγ expression is induced by SBRT/IL-12mRNA and is essential to treatment efficacy

(A) Tumor IFNγ concentration measured by luminex at 24 h and 96 h post IL-12mRNA injection. (B) IFNγ+ CD4 and CD8 T cells at 24 h and 72 h post IL-12mRNA injection. (C) UMAPs for CD4 and CD8 T cells for each treatment group depicting levels of IFNγ gene expression. (D) SBRT/IL-12mRNA efficacy in IFNγ KO vs. wild-type mice. (E) Proliferation and frequency of CD4 and CD8 T cells in IFNγ KO vs. wild-type mice following SBRT/IL-12mRNA treatment. n = 5/group from two independent experiments in (A). n = 10/group from two independent experiments. n = 5/group in (D) and (E). One-way ANOVA followed by Tukey's test. Significance against untreated and between treatments are reported. *$p < 0.05$; **$p < 0.01$; ****$p < 0.0001$. Lines represent mean ± SEM for (A), (B), (D) and (E).

IFNγ was shown to be indispensable in this model as treatment efficacy was completely lost when KP2 tumors grown in IFNγ$^{-/-}$ mice failed to respond to SBRT/IL-12mRNA therapy (Figure 7D). We utilized these transgenic mice to assess whether the robust proliferation signature described in Figure 4 was linked to IFNγ production. Either WT or IFNγ$^{-/-}$ mice bearing KP2 and treated as in Figure 1A were administered BrdU 4 h before they were euthanized and incorporation was examined by flow cytometry. Interestingly, CD4 and CD8 intratumoral T cells from *both* WT and IFNγ$^{-/-}$ mice incorporated BrdU to a similar extent suggesting that intratumoral T cells were able to proliferate without IFNγ (Figure 7E, upper left and right, respectively). This proliferation still leads to an increased density of intratumoral CD4 T cells regardless of the presence or absence of IFNγ following SBRT/IL-12mRNA therapy (Figure 7E, bottom left), however failed to augment the already basally low CD8 T cell density in IFNγ$^{-/-}$ mice (Figure 7E, bottom right). Collectively, these data demonstrate that IFNγ, produced predominantly by intratumoral CD4 and CD8 Intermediate and Activated/Cycling T cell populations after SBRT/IL-12mRNA, are required to mediate treatment efficacy.

DISCUSSION

Chronic antigen exposure along with TME suppressive cues can render T cells to adopt a dysfunctional state known as exhaustion.[20] Immune checkpoint blockade (ICB), which has revolutionized cancer immunotherapy, predominately acts to reverse T cell exhaustion and reinvigorate the adaptive immune response.[21] One striking finding from our work was that SBRT/IL-12mRNA resembled ICB in that intratumoral T cells exhibited an activated/effector phenotype that coincided with an absence of exhausted cells. Although the combination of SBRT and IL-12mRNA resulted in the most profound ratio of activated to exhausted T cells, it was clear that this effect was largely attributed to the presence of intratumoral IL-12 (Figures 4C and 4D). It is well established that IL-12 has direct effects including induction of proliferation[22,23] and effector function,[24] and paramount to this discussion, reversal of T cell exhaustion.[25] Work by Tucker et al. demonstrated that preconditioning adoptively transferred T cells with IL-12 reduced the exhaustion transcription factor Tox and surface expression of Lag3.[26] Additionally, CAR T cells, which are frequently rendered ineffective due to exhaustion, have been shown to overcome this suppressive phenotype by genetic engineering to constitutively express IL-12.[27] Similar results have also been achieved for tumor-residing T cells utilizing novel means for local delivery of IL-12 via fusion proteins to target fibronectin,[28] collagen,[29–32] and matrix metalloproteases.[33] These previous reports have demonstrated the ability of IL-12 to directly act upon a non-terminally differentiated exhausted T cell and convert it to an effector cell. It is likely that this mechanism is contributing to the T cell conversion in our model. However, another scenario exists in that radiosensitive intratumoral T cells could be reduced by SBRT.[34] These basal state T cells would be an exhausted phenotype and essentially deleted from the TME following radiotherapy, thereby clearing a niche and opening up space for new T cell repopulation. In essence, SBRT may wipe the slate clean allowing for the influx of new T cells that are not yet exhausted and can be strongly polarized toward an activated/effector phenotype by (1) an inflammatory milieu of cytokines and danger-associated molecular patterns (DAMPs) released by SBRT, and (2) concentrated IL-12 in the TME. In such a case, the scheduling and order of therapy would be essential, requiring SBRT to be given before administration of local IL-12, which would allow for the depletion of exhausted cells, rather than the IL-12-activated T cells.

A robust proliferative signature was observed in the Activated/Cycling T cells from SBRT/IL-12mRNA-treated tumors, which represented over half of all intratumoral T cells. Notably, over 1,000 DEGs were identified in this cluster. A major subset of these genes centered around proliferation and cell division, and were the driving factor in determining UMAP position of the subclustered T cells when analyzed by vector analysis. We were surprised by the limited expression of effector genes in this specific population. One reason for this finding may be linked to the high metabolic demand required for cells undergoing proliferation.[35] Cell division imposes a profound strain on energy consumption as each passage through cell cycle requires the complete doubling of all biomass (macromolecules, lipids, nucleic acids, proteins, etc.) resulting in two daughter cells.[36,37] This process requires a major reorganization of the cellular metabolic activities allowing the cell to shunt energy into pathways that ultimately support cell division. It is possible that energy is transiently "borrowed" from effector pathways resulting in the observed diminished expression of these genes. Regardless, the SBRT/IL-12mRNA tumors were not devoid of T cells that expressed an effector phenotype. On the contrary, the Intermediate population highly expressed effector associated genes such as IFNγ, granzymes, perforin, etc., but demonstrated a low proliferative signature. The trajectory analysis linked the Activated/Cycling and Intermediate populations together, but intriguingly did not show a terminal population within the activated/cycling cluster. We propose that an external stimuli consisting of IL-12 and other yet unknown factors initiate robust T cell proliferation (the Activated/Cycling population) that when completed, gives rise to a large population of T cells with the capacity to reactivate effector function to elicit antitumor activity (the Intermediate population). This concept is intriguing as it suggests that a unique milieu of SBRT/IL-12mRNA-induced factors can support *intratumoral* T cell expansion, an anatomical location not typically considered as being hospitable to support T cell division.

Historically, IL-12 and IFNγ have been linked as potent inducers of T cell proliferation. Some publications attribute this characteristic as a direct effect of IL-12 through a STAT4-mediated mechanism,[22,38] whereas others highlight the importance of IFNγ stimulating T cell division.[39,40] In our model, the frequency of intratumoral proliferating T cells (as assessed by BrdU incorporation) was essentially identical between WT and IFNγKO mice. These data suggest that IL-12 alone (or IL-12-induced factors) were driving T cell proliferation independent of IFNγ. Importantly, all treatment efficacy was lost in IFNγKO mice even though proliferation was intact. This suggests

that T cell proliferation without IFNγ renders these T cells completely ineffective in this model. Therefore, what essential role is IFNγ having? The answer likely lies in the difference between the Activated/Cycling and the Intermediate population as described above. The Activated/Cycling cells are dividing but express little IFNγ and a muted effector phenotype, whereas IFNγ is more abundant, along with effector genes, in the Intermediate population. The IFNγKO mice have proliferating T cells, but poor effector function, emphasizing the importance of this Intermediate population in mediating tumor cell killing. Other antitumor roles for IFNγ presumably exist. The vast majority of IFNγ was produced by T cells allowing for autocrine stimulation (or paracrine from CD4 T cells) of cytolytic capabilities of CD8 T cells. IFNγ is well established to act on intratumoral cells such as tumor, stromal, endothelial, and myeloid cells often promoting antitumor activity.[41] Distally in the draining lymph node, we demonstrated Tbet induction; evidence of a strong induction to a Th1 response driven by IL-12-induced IFNγ. Collectively, T cell proliferation is important to expand intratumoral T cell populations; however, IFNγ licenses them to become effector T cells and ultimately eliminate the tumor.

Although SBRT has been shown to downstage locally advanced or borderline resectable tumors in PDAC patients,[42] it rarely results in a complete clinical response or long-term survival. We observed similar results in our preclinical model as SBRT alone had minimal effects on tumor burden and survival; however, when combined with IL-12, could completely eliminate disease. Therefore, what is the contribution of SBRT to this therapy? We have demonstrated both preclinically[18,43] and clinically[44] that SBRT induces immunogenic cell death of tumor cells with subsequent release of DAMPs such as HMGB1, HSP70, and calreticulin. In cancer, DAMPs bind to cellular cognate receptors to sense damage/danger in the TME, which, in turn, stimulates proinflammatory cytokine release such as Type I IFNs.[45] This cascade of events is essential to initiate antitumor immune responses. Dendritic cells are the predominate immune subset that react to DAMPs; however, "bystander" T cells also respond to these molecules through TLR, and this promotes T cell activation in a TCR-independent manner.[46,47] There is evidence in our model that SBRT is also stimulating a response to DAMPs as a strong Type I IFN signature is observed in macrophages, monocytes, and DCs (Figure S6). Another possibility is that SBRT augments the concentration of IL-12 in both the tumor and dLN (Figures S2A and S2B), thereby providing a potential beneficial effect. We tested whether the uptake or translation of IL-12mRNA is enhanced in irradiated tumor cells *in vitro*; however, no differences were observed (data not shown). It is possible that *endogenous* production of IL-12 is increased with the addition of SBRT and/or SBRT modulates the number of the cellular producers of exogenous IL-12 *in vivo*. Either possibility would lead to an increase in intratumoral IL-12 concentration mediated by SBRT. Additionally, a likely attribute of SBRT is its ability to reshape the TCR repertoire. The optimal antitumor T cell response would be to generate clonal expansion against numerous tumor antigens. We have shown that SBRT increased expansion of the top 1% clonotypes, which likely translates into extended coverage of the TCR repertoire against more tumor antigens. We propose that SBRT exposes and releases novel tumor antigens that would otherwise not be recognized by the immune system without this treatment modality. Typically, this is the point where the expanded repertoire of T cells would possess TCRs that specifically recognize tumor cells, only to be suppressed by the PDAC TME via checkpoint molecules and/or induction of exhaustion. However, intratumoral IL-12 prevents this suppression and instead, promotes robust proliferation and effector function of these tumor-specific T cells directly at the tumor site. In essence, the combination of SBRT and IL-12mRNA evokes T cell proliferation against a diverse set of tumor antigens that do not become exhausted and go on to eliminate the pancreatic tumor.

Abscopal effects capable of eliminating liver metastases were observed when SBRT and IL-12mRNA were delivered to pancreas tumors. While the mechanisms behind this systemic immunity have not been explored here, it can be speculated that the potent antitumor immune responses responsible for overcoming primary tumors may also be efficacious in distal lesions. Increases in IL-12 (Figure S2B), IFNγ, and Tbet (Figures S12A–S12C) were observed distally in the tumor dLN and are known to be key mediators of antitumor immunity. It is likely that each of these factors contributes to abscopal effects observed here.

The data presented here demonstrate that local administration of SBRT and IL-12mRNA essentially propels every cell in the TME toward an antitumor state. This "sledgehammer" approach is capable of rejecting primary tumors, but also stimulates a systemic response that eliminates distal hepatic metastases. SBRT is already an approved standard of care for PDAC patients. Intratumoral administration of antitumor therapeutics is an emerging field as investigators explore non-systemic means to introduce drugs directly to the tumor. Endoscopic ultrasound-guided biopsy is routinely used in PDAC,[48] and can be repurposed to deliver immunotherapeutics such as IL-12mRNA. Importantly, the human equivalent of this construct (MEDI1191) has already undergone a phase I clinical study across multiple solid malignancies including pancreatic cancer (NCT03946800) and proven safe and tolerable, even with multiple intratumoral doses of the therapy given (up to 3 μg per dose).[8] Collectively, this work represents evidence that even the recalcitrant PDAC TME can be overpowered when the correct combination of therapies (in this case SBRT and IL-12mRNA) are administered locally.

MATERIALS AND METHODS

In vivo animal studies

Female 6- to 8-week-old C57BL/6J and B6.129S7-Ifng^{tm1Ts}/J (IFNg$^{-/-}$) mice were purchased from The Jackson Laboratory. P48-Cre$^{+/-}$; Tp53 $^{L/L}$ and LSL-Kras^{G12D} mice were obtained from Dr. Aram Hezel and crossed to generate the LSL-Kras^{G12D}; Tp53$^{L/L}$; P48-Cre; (KPC) genotype.[14,49] All experiments were approved by the University Committee on Animal Resources and

were performed in compliance with the NIH and University of Rochester-approved guidelines for the care and use of animals.

Cell lines

KP2 (derived from KPC mice) and KCKO (derived from KC mice; LSL-Kras^{G12D}; P48-Cre) cell lines stably express firefly luciferase and were provided by Dr. David DeNardo.[50] Both cell lines were cultured in MAT/P (US patent No. 4.816.401) supplemented with 5% fetal bovine serum (Hyclone) and 1% penicillin/streptomycin (GIBCO) and incubated at 37°C, 5% CO_2.

Orthotopic tumor mouse model

Mice were anesthetized using vaporized isoflurane (Scivena Scientific) and a 10-mm laparotomy incision was made to expose the spleen and pancreas. KP2.1-luc (2.5×10^4) or KCKO-luc (5×10^4) cells were resuspended in a 1:1 PBS:Matrigel (Corning) solution and injected into the tail of the pancreas (40 μL volume). Two 4-mm titanium fiducial clip markers (Horizon) were implanted adjacent to the Matrigel bubble to assist in SBRT targeting. The peritoneal cavity was then sutured with 4-0 VICRYL SH-1 (eSutures) and skin was stapled using 9-mm wound clips (Reflex).

Metastasis model

Mice were anesthetized using vaporized isoflurane and a 20-mm laparotomy incision was made to expose the abdominal cavity. The hepatic portal vein was exposed and 1×10^5 KP2.1-luc cells in 100 μL of PBS was injected into the vein using a 30-gauge Hamilton syringe to establish hepatic metastasis. Concurrently, primary pancreatic tumors were injected as described above. The peritoneum was sutured and skin stapled as before.

Radiation therapy

All radiation was delivered using the Small Animal Radiation Research Platform (SARRP, XStrahl) equipped with a computed tomography (CT) scanning device (Muriplan software) as described previously.[7] Briefly, tumor-bearing mice were anesthetized with vaporized isoflurane and transferred to the SARRP. Pancreatic tumors were identified by a CT image based on two titanium fiducial clips placed on either side of the tumor at the time of tumor injection. SBRT was administered to the tumor following a dosing schedule of four fractions each consisting of 6 Gy radiation on days 6–9 post-implantation.

IL-12mRNA injection

IL-12mRNA and scr-mRNA lipid nanoparticles were provided by Moderna Inc. and their synthesis and design have been described previously.[9] Briefly, the IL-12mRNA encoded sequences for wild-type mouse IL12α and IL12β subunits joined by a polypeptide linker to generate a stable IL12p70 fusion protein incorporating N1-methyl-pseudouridine and miR122 modifications as reported elsewhere.[51] scr-mRNA (control for IL-12mRNA) was modified to exclude an initiating codon and therefore is non-translating. Twenty-four hours after the final SBRT fraction (day 10 post tumor implantation), mice were anesthetized with vaporized isoflurane and a 10-mm laparotomy incision was made to expose the pancreas and tumor. scr-mRNA or IL-12mRNA (0.5 μg in 25 μL) was injected intratumorally using a 30-gauge Hamilton syringe.

Bioluminescent imaging

In vivo tumor growth was measured using the *In Vivo* Imaging Systems (IVIS, PerkinElmer). Tumor-bearing mice were anesthetized and injected subcutaneously (s.c.) with D-luciferin (2.5 mg/100 μL PBS, Invitrogen). Mice were placed in a right lateral recumbent position and a series of 12 consecutive images were taken at 2-min intervals. Bioluminescent imaging (BLI) (p/sec/cm^2/sr) was calculated within matching (circular) regions of interest (ROIs) manually placed over tumors. Peak intensity was recorded for each tumor and used as a readout of tumor burden.

Rechallenge model

Mice were injected with orthotopic tumors and treated with SBRT and IL-12mRNA as described above. Six weeks after IL-12mRNA injection (4 weeks after loss of BLI signal), mice were rechallenged systemically with an injection of 1×10^5 KP2-luc cells through the hepatic portal vein as described above. Additionally, treatment-naïve aged-matched mice were also injected at the same time as controls.

Flow cytometry

Tumors were mechanically dissociated on days 1, 3, and 7 post IL-12mRNA/scr-mRNA injection (days 11, 13, and 17 post inoculation) and digested in 30% collagenase (Sigma) for 30 min at 37°C. Homogenates were then passed through a 70-μm filter to generate a single-cell suspension that was redispersed in PBS containing 1% bovine serum albumin and 0.1% sodium azide. This suspension was then stained for various markers.

To assess immune populations in tumors, single-cell suspensions were stained with the following: Ghost Dye 510 (Tonbo), CD4-BUV395 (RM4-5, BD), CD11b-AF700 (M1/70, Biolegend), F4/80-APC (BM8, Life Technologies), Ly6C-PEcy7 (HK1.4, Biolegend), CD8-PEcy5 (53–6.7, BD), NK1.1-PECF595 (PK136, BD), CD45-PerCPcy5.5 (30-f11, BD), CD19-BV786 (ID3, BD), CD11c-BV711 (HL3, BD), Ly6G-BV650 (IA8, Biolegend), TCRγδ-BV605 (GL3, Biolegend), IFNγ-PE (XMG1.2, Biolegend), and Foxp3-APC (FJK-16s, eBioscience). For intercellular staining of IFNγ, BD Cytofix/Cytoperm Plus kit (BD) was used.

For macrophage activation analysis, cells were stained with CD45-BUV395 (30-F11, BD), CD11b-EF450 (M1/70, Invitrogen), F4/80-AF488 (BM8, Biolegend), Arg-1-AF700 (A1exF5, eBioscience), IA/IE-PerCP/Cy5.5 (M5.114.15.2, Biolegend), H2Kb-APC (AF6.88.5, Biolegend), CD206-BV785 (C068C2, Biolegend), CD163-PE-Dazzle594 (S15049F, Biolegend), PDL1-BV605 (10F.PG2, Biolegend), and IFNγ-PE (XMG1.2, Biolegend).

For T cell proliferation analysis, 1 mg of 5-bromo-2-deoxyuridine (BrdU) was injected intraperitoneally 4 h prior to tumor harvest on

day 13 post tumor inoculation (3 days post IL-12mRNA/scRNA treatment). Cells were then stained according to BrdU APC staining kit instructions (BD).

All samples were run on an LSRII Fortessa (BD Bioscience) and analyzed using FlowJo software.

Single-cell RNA sequencing

For scRNA-seq, 2 KP2.1 tumors were pooled per treatment group at 3 days post IL-12mRNA/scr-mRNA injection (day 13 post tumor inoculation), minced, and digested in collagenase (Sigma) for 30 min at 37°C. Single-cell suspensions were stained with Ghost Dye 510 (Tonbo). Live singlet cells were sorted using the FACSAria II (BD) using a 100-μm nozzle and provided to the University of Rochester Genomics Research Center for RNA purification, sequencing and analysis. scRNA-seq libraries were generated using Chromium Single-Cell (10x Genomics) according to the manufacturer's instructions with a target cell capture of 10k cells per sample and 100k reads per cell.

Libraries were sequenced on Illumina NovaSeq 6000 sequencer. Raw sequencing data were processed using Cell Ranger (v6.0.1) and aligned to mouse reference genome GRCm38.

Quality control was performed using Seurat (version 4.2.0) by removing cells with low-quality RNA based on high mitochondrial gene content (percent mt > 20%), or low unique gene counts (nFeature <200). To avoid doublets, cells with more than 6,500 feature counts were also excluded. The remaining cells were normalized, anchor-point analysis performed, and merged according to Seurat pipeline guidelines to form a combined seurat object for downstream analysis.

Cell clustering and differential analysis were performed via the Seurat pipeline using the Louvain algorithm. Clusters were annotated using known marker genes and manual inspection of cluster-specific gene expression patterns based on positive expression and minimum percentage expression by cluster greater than 25%. Secondary automated classification was performed using sc-Type for cross comparison. Differential expression analysis was conducted using a Wilcoxon rank-sum test using an adjusted p value (Bonferroni false discovery rate) threshold of 0.05. Cluster comparisons were made as specified in the text either between manual cluster classification for all cells in that cluster of the merged seurat object and/or by cluster classification subset by condition of origin.

For subset analysis, CD4 and CD8 seurat objects were subset on CD3e > 1.0 and CD4 > 0.5 or CD8a >1.0, respectively. Pseudotime trajectories were generated using Monocle3 (Version 1.3.1) using manually identified naive T cells as the root population for each seurat object.

TCR sequencing

For TCR sequencing (TCR-seq), 5 KP2.1 tumors were pooled per treatment group 3 days post IL-12mRNA/scr-mRNA injection (day 13 post tumor inoculation), minced, and digested in collagenase (Sigma) for 30 min at 37°C. Single-cell suspensions were stained with Ghost Dye 510 (Tonbo), CD45-PerCPcy5.5 (30-f11, BD), CD4-BV605 (RM4-5, BD), and CD8-PEcy5 (53–6.7, BD). Cells were sorted into two populations, CD4+ and CD8+, using a FACSAria II (BD) using a 100-μm nozzle. Cells were immediately lysed in RLT Plus buffer (Qiagen) and delivered to the University of Rochester Genomics Research Center for sequencing and analysis.

TCR-seq data were run through MiXCR (MiLabs) using a pipeline for analysis of enriched targeted TCR libraries. The pipeline performed alignment of raw sequencing reads, assembly of aligned sequences into clonotypes, and output of the resulting clonotypes into tab-delimited files. The final list of clones was further analyzed using Seurat and Immunarch in R. TCR clones were downsized randomly to the lowest number of clones in the four groups (untreated, SBRT, IL-12mRNA, SBRT/IL-12mRNA). Clonotypes were defined as the set of all TCR clones with the same CDR3 nucleic acid sequence. High clonality indicates fewer overall clonotypes, with each clonotype having a higher frequency. Low clonality indicates the even distribution of clonotypes across the repertoire. Chao1 diversity was calculated using Immunarch in R. Bubble plots displaying the top 1% of clonotypes in each TCR repertoire were generated using Seurat. The size of each bubble corresponds to the number of clones with that clonotype. The average size of the bubbles in each plot was calculated and plotted.

Antibody depletion

Depleting antibodies were administered (200 μg in 100 μL PBS) subcutaneously beginning on day 5 post KP2.1 tumor implantation (1 day before SBRT begins) and continued every 3 days for a total of seven doses. The antibodies (Bio X Cell) administered were rat isotype control (clone 2A3), rat anti-mouse CD8a (clone 53.6.7), rat anti-mouse CD4 (clone GK1.5), anti-mouse NK1.1 (clone PK136), and mouse isotype control (clone C1.18.4).

Immunohistochemistry

Three days post IL-12mRNA/scr-mRNA injection (day 13 post-implantation) KP2.1 tumors were harvested, paraffin embedded, and 5-μm tumor sections were stained with hematoxylin and eosin (H&E). Slides were analyzed in a blinded fashion by a board-certified pathologist. Images are representative of three individual tumors for each treatment group.

Luminex assay

KP2.1 tumor, draining lymph node (dLN), non-draining lymph node (ndLN), and liver were harvested 1 day or 4 days post IL-12mRNA/scr-mRNA injection (day 11 or 14 post inoculation), homogenized, and digested in Cell Lysis Buffer #2 (R&D Systems) containing protease inhibitors on ice for 1 h. The samples were centrifuged at 14,000 rpm for 20 min at 4°C and supernatants were collected. Magnetic Luminex Assays were preformed using a Mouse Premixed Cytokine/Chemokine Multi-Analyte kit (R&D Systems) according to the manufacturer's instructions. Microplates were run on a

Bio-Plex 200 system (Bio-Rad). Total protein concentrations for each sample were calculated using Pierce BCA Protein Assays (Thermo Fisher Scientific) and used for analyte normalization into pg/mg protein values.

Blood biochemistry

Mice were inoculated with KP2.1 tumors and treated as before. Three days or 14 days post IL-12mRNA/scr-mRNA injection, mice were euthanized via cardiac perfusion and serum isolated and frozen at −80°C for subsequent analysis. Naive, non-tumor-bearing aged-matched serum were used as controls. Blood biochemical analysis for liver and kidney functional markers was performed by IDEXX BioAnalytics.

ELISA and qPCR

In vitro cultured cells, KP2, mouse embryonic fibroblasts (MEFs), naive CD4/CD8 lymphocytes and peritoneal lavage macrophages, were treated with IL12mRNA or scr-mRNA for 24 h. Supernatants were assayed for IL-12 protein with the Murine IL-12 Standard ELISA Development Kit (Peprotech) according to manufacturer's instructions. RNA was isolated from the cells using the RNeasy Plus Mini Kit (Qiagen), cDNA was then generated with the iScript cDNA Synthesis Kit (Bio-Rad) according to manufacturer's instructions. The protocol from IDT, Prime Time qPCR Assay reactions (Premixed primer and probes) was followed to assay for a unique sequence in IL-12mRNA using the CFX96 Real-Time System (C1000 Thermocycler, Bio-Rad).

Statistical analysis

GraphPad Prism 9 software was used for all statistical analyses and p values of <0.05 were considered significant. BLI growth curves used the geometric mean of maximum photon emissions for each time point and treatment group from a single ROI. Growth curve significance was assessed using ANOVA followed by Dunn's multiple comparison test. For survival analysis, Mantel-Cox tests were performed. Rechallenge studies were analyzed by Mann-Whitney test. Reported significance was against the untreated group, unless otherwise stated.

DATA AND CODE AVAILABILITY

The data generated in this study are available upon request from the corresponding author. Transcriptomic data in this study is publicly available in the Gene Expression Omnibus (GEO) at GSE242111.

ACKNOWLEDGMENTS

We would like to acknowledge Mary Georger from the Histology Core, and Eric Hernady from the Small Animal Irradiation Core, as well as the Genomics Research Center and Flow Cytometry Core at URMC for their help with this article. Support for mRNA manufacture and lipid nanoparticle formulation was provided by Moderna Inc, Cambridge, MA, USA. Biorender software was used for the creation of all figures and the graphical abstract.

Funding: NCI Grants R01CA236390, R01CA230277, R01CA262580; NIH Grant AI007285. Supported by grants from the NCI (R01CA230277 to S.A.G., and R01CA262580 to S.A.G. and D.C.L.), NIH (AI007285 to T.G.V.), and AstraZeneca.

AUTHOR CONTRIBUTIONS

A.L.H., G.H., N.A.S., T.G.V., C.A.S., B.N.M., J.G.-L., C.J.J., J.D.M., E.K., J.Y., N.W.G., D.C.K., S.S.Q., and M.L.L. conducted experiments. A.L.H., G.H., N.A.S., T.G.V., B.N.M., H.Q., C.J.J., J.D.M., J.B.M., T.M.T.L., L.M.C., E.M.L., N.L., J.E., D.C.L., and S.A.G. were involved in conceptualization. A.L.H., G.H., and S.A.G. wrote the manuscript. A.L.H. and G.H. contributed equally. Statistical analysis: T.M.T.L.

DECLARATION OF INTERESTS

This research was funded in-part by AstraZeneca. N.L. and J.E. are both employees at AstraZeneca and own stocks and shares.

SUPPLEMENTAL INFORMATION

Supplemental information can be found online at https://doi.org/10.1016/j.omtn.2024.102350.

REFERENCES

1. Thommen, D.S., and Schumacher, T.N. (2018). T Cell Dysfunction in Cancer. Cancer Cell *33*, 547–562.
2. Jiang, Y., Li, Y., and Zhu, B. (2015). T-cell exhaustion in the tumor microenvironment. Cell Death Dis. *6*, e1792.
3. Karasarides, M., Cogdill, A.P., Robbins, P.B., Bowden, M., Burton, E.M., Butterfield, L.H., Cesano, A., Hammer, C., Haymaker, C.L., Horak, C.E., et al. (2022). Hallmarks of Resistance to Immune-Checkpoint Inhibitors. Cancer Immunol. Res. *10*, 372–383.
4. Habiba, U.E., Rafiq, M., Khawar, M.B., Nazir, B., Haider, G., and Nazir, N. (2022). The multifaceted role of IL-12 in cancer. Adv. Cancer Biol. Metast. *5*, 100053.
5. Atkins, M.B., Robertson, M.J., Gordon, M., Lotze, M.T., DeCoste, M., DuBois, J.S., Ritz, J., Sandler, A.B., Edington, H.D., Garzone, P.D., et al. (1997). Phase I evaluation of intravenous recombinant human interleukin 12 in patients with advanced malignancies. Clin. Cancer Res. *3*, 409–417.
6. Gollob, J.A., Mier, J.W., Veenstra, K., McDermott, D.F., Clancy, D., Clancy, M., and Atkins, M.B. (2000). Phase I trial of twice-weekly intravenous interleukin 12 in patients with metastatic renal cell cancer or malignant melanoma: ability to maintain IFN-gamma induction is associated with clinical response. Clin. Cancer Res. *6*, 1678–1692.
7. Mills, B.N., Connolly, K.A., Ye, J., Murphy, J.D., Uccello, T.P., Han, B.J., Zhao, T., Drage, M.G., Murthy, A., Qiu, H., et al. (2019). Stereotactic Body Radiation and Interleukin-12 Combination Therapy Eradicates Pancreatic Tumors by Repolarizing the Immune Microenvironment. Cell Rep. *29*, 406–421.e5.
8. Castañón, E., Zamarin, D., Carneiro, B.A., Marron, T., Patel, S.P., Subbiah, V., Mehmi, I., Oberoi, H.K., El-Khoueiry, A., Ridgway, B., et al. (2023). Abstract CT004: Intratumoral (IT) MEDI1191 + durvalumab (D): Update on the first-in-human study in advanced solid tumors. Cancer Res. *83*, CT004.
9. Hewitt, S.L., Bailey, D., Zielinski, J., Apte, A., Musenge, F., Karp, R., Burke, S., Garcon, F., Mishra, A., Gurumurthy, S., et al. (2020). Intratumoral IL12 mRNA Therapy Promotes TH1 Transformation of the Tumor Microenvironment. Clin. Cancer Res. *26*, 6284–6298.
10. Li, H.-B., Yang, Z.-H., and Guo, Q.-Q. (2021). Immune checkpoint inhibition for pancreatic ductal adenocarcinoma: limitations and prospects: a systematic review. Cell Commun. Signal. *19*, 117.
11. Tchelebi, L.T., Lehrer, E.J., Trifiletti, D.M., Sharma, N.K., Gusani, N.J., Crane, C.H., and Zaorsky, N.G. (2020). Conventionally fractionated radiation therapy versus stereotactic body radiation therapy for locally advanced pancreatic cancer (CRiSP): An international systematic review and meta-analysis. Cancer *126*, 2120–2131.
12. van Goor, I.W.J.M., Daamen, L.A., Besselink, M.G., Bruynzeel, A.M.E., Busch, O.R., Cirkel, G.A., Groot Koerkamp, B., Haj Mohammed, N., Heerkens, H.D., van Laarhoven, H.W.M., et al. (2022). A nationwide randomized controlled trial on additional treatment for isolated local pancreatic cancer recurrence using stereotactic body radiation therapy (ARCADE). Trials *23*, 913.
13. Kim, M.P., Li, X., Deng, J., Zhang, Y., Dai, B., Allton, K.L., Hughes, T.G., Siangco, C., Augustine, J.J., Kang, Y., et al. (2021). Oncogenic KRAS Recruits an Expansive Transcriptional Network through Mutant p53 to Drive Pancreatic Cancer Metastasis. Cancer Discov. *11*, 2094–2111.

14. Hingorani, S.R., Wang, L., Multani, A.S., Combs, C., Deramaudt, T.B., Hruban, R.H., Rustgi, A.K., Chang, S., and Tuveson, D.A. (2005). Trp53R172H and KrasG12D cooperate to promote chromosomal instability and widely metastatic pancreatic ductal adenocarcinoma in mice. Cancer Cell *7*, 469–483.

15. UCLA (2013). Serum Chemistry Reference Range - Mouse. https://labs.dgsom.ucla.edu/dlam/files/view/docs/diagnostic-lab-services/private/serum_chemistry_reference_ranges_mice.pdf.

16. Yousuf, S., Qiu, M., Voith von Voithenberg, L., Hulkkonen, J., Macinkovic, I., Schulz, A.R., Hartmann, D., Mueller, F., Mijatovic, M., Ibberson, D., et al. (2023). Spatially Resolved Multi-Omics Single-Cell Analyses Inform Mechanisms of Immune Dysfunction in Pancreatic Cancer. Gastroenterology *165*, 891–908.e14.

17. Chow, J., Hoffend, N.C., Abrams, S.I., Schwaab, T., Singh, A.K., and Muhitch, J.B. (2020). Radiation induces dynamic changes to the T cell repertoire in renal cell carcinoma patients. Proc. Natl. Acad. Sci. USA *117*, 23721–23729.

18. Ye, J., Mills, B.N., Qin, S.S., Garrett-Larsen, J., Murphy, J.D., Uccello, T.P., Han, B.J., Vrooman, T.G., Johnston, C.J., Lord, E.M., et al. (2022). Toll-like receptor 7/8 agonist R848 alters the immune tumor microenvironment and enhances SBRT-induced antitumor efficacy in murine models of pancreatic cancer. J. Immunother. Cancer *10*, e004784.

19. Liu, J., Cao, S., Kim, S., Chung, E.Y., Homma, Y., Guan, X., Jimenez, V., and Ma, X. (2005). Interleukin-12: an update on its immunological activities, signaling and regulation of gene expression. Curr. Immunol. Rev. *1*, 119–137.

20. Wherry, E.J. (2011). T cell exhaustion. Nat. Immunol. *12*, 492–499.

21. Budimir, N., Thomas, G.D., Dolina, J.S., and Salek-Ardakani, S. (2022). Reversing T-cell Exhaustion in Cancer: Lessons Learned from PD-1/PD-L1 Immune Checkpoint Blockade. Cancer Immunol. Res. *10*, 146–153.

22. Yoo, J.K., Cho, J.H., Lee, S.W., and Sung, Y.C. (2002). IL-12 provides proliferation and survival signals to murine CD4+ T cells through phosphatidylinositol 3-kinase/Akt signaling pathway. J. Immunol. *169*, 3637–3643.

23. Kieper, W.C., Prlic, M., Schmidt, C.S., Mescher, M.F., and Jameson, S.C. (2001). IL-12 Enhances CD8 T Cell Homeostatic Expansion. J. Immunol. *166*, 5515–5521.

24. Braun, M., Ress, M.L., Yoo, Y.E., Scholz, C.J., Eyrich, M., Schlegel, P.G., and Wölfl, M. (2016). IL12-mediated sensitizing of T-cell receptor-dependent and -independent tumor cell killing. OncoImmunology *5*, e1188245.

25. Schurich, A., Pallett, L.J., Lubowiecki, M., Singh, H.D., Gill, U.S., Kennedy, P.T., Nastouli, E., Tanwar, S., Rosenberg, W., and Maini, M.K. (2013). The Third Signal Cytokine IL-12 Rescues the Anti-Viral Function of Exhausted HBV-Specific CD8 T Cells. PLoS Pathog. *9*, e1003208.

26. Tucker, C.G., Mitchell, J.S., Martinov, T., Burbach, B.J., Beura, L.K., Wilson, J.C., Dwyer, A.J., Singh, L.M., Mescher, M.F., and Fife, B.T. (2020). Adoptive T Cell Therapy with IL-12-Preconditioned Low-Avidity T Cells Prevents Exhaustion and Results in Enhanced T Cell Activation, Enhanced Tumor Clearance, and Decreased Risk for Autoimmunity. J. Immunol. *205*, 1449–1460.

27. Yeku, O.O., Purdon, T.J., Koneru, M., Spriggs, D., and Brentjens, R.J. (2017). Armored CAR T cells enhance antitumor efficacy and overcome the tumor microenvironment. Sci. Rep. *7*, 10541.

28. Ongaro, T., Matasci, M., Cazzamalli, S., Gouyou, B., De Luca, R., Neri, D., and Villa, A. (2019). A novel anti-cancer L19-interleukin-12 fusion protein with an optimized peptide linker efficiently localizes in vivo at the site of tumors. J. Biotechnol. *291*, 17–25.

29. Momin, N., Mehta, N.K., Bennett, N.R., Ma, L., Palmeri, J.R., Chinn, M.M., Lutz, E.A., Kang, B., Irvine, D.J., Spranger, S., and Wittrup, K.D. (2019). Anchoring of intratumorally administered cytokines to collagen safely potentiates systemic cancer immunotherapy. Sci. Transl. Med. *11*, eaaw2614.

30. Mansurov, A., Ishihara, J., Hosseinchi, P., Potin, L., Marchell, T.M., Ishihara, A., Williford, J.M., Alpar, A.T., Raczy, M.M., Gray, L.T., et al. (2020). Collagen-binding IL-12 enhances tumour inflammation and drives the complete remission of established immunologically cold mouse tumours. Nat. Biomed. Eng. *4*, 531–543.

31. Li, Y., Su, Z., Zhao, W., Zhang, X., Momin, N., Zhang, C., Wittrup, K.D., Dong, Y., Irvine, D.J., and Weiss, R. (2020). Multifunctional oncolytic nanoparticles deliver self-replicating IL-12 RNA to eliminate established tumors and prime systemic immunity. Nat. Cancer *1*, 882–893.

32. Kang, S., Mansurov, A., Kurtanich, T., Chun, H.R., Slezak, A.J., Volpatti, L.R., Chang, K., Wang, T., Alpar, A.T., Refvik, K.C., et al. (2023). Engineered IL-7 synergizes with IL-12 immunotherapy to prevent T cell exhaustion and promote memory without exacerbating toxicity. Sci. Adv. *9*, eadh9879.

33. Xue, D., Moon, B., Liao, J., Guo, J., Zou, Z., Han, Y., Cao, S., Wang, Y., Fu, Y.X., and Peng, H. (2022). A tumor-specific pro-IL-12 activates preexisting cytotoxic T cells to control established tumors. Sci. Immunol. *7*, eabi6899.

34. Gough, M.J., and Crittenden, M.R. (2022). The paradox of radiation and T cells in tumors. Neoplasia *31*, 100808.

35. Buck, M.D., O'Sullivan, D., and Pearce, E.L. (2015). T cell metabolism drives immunity. J. Exp. Med. *212*, 1345–1360.

36. DeBerardinis, R.J., Lum, J.J., Hatzivassiliou, G., and Thompson, C.B. (2008). The Biology of Cancer: Metabolic Reprogramming Fuels Cell Growth and Proliferation. Cell Metab. *7*, 11–20.

37. Zhu, J., and Thompson, C.B. (2019). Metabolic regulation of cell growth and proliferation. Nat. Rev. Mol. Cell Biol. *20*, 436–450.

38. Schaller, M., Ito, T., Allen, R.M., Kroetz, D., Kittan, N., Ptaschinski, C., Cavassani, K., Carson, W.F., 4th, Godessart, N., Grembecka, J., et al. (2015). Epigenetic regulation of IL-12-dependent T cell proliferation. J. Leukoc. Biol. *98*, 601–613.

39. Siegel, J.P. (1988). Effects of interferon-γ on the activation of human T lymphocytes. Cell. Immunol. *111*, 461–472.

40. Whitmire, J.K., Tan, J.T., and Whitton, J.L. (2005). Interferon-γ acts directly on CD8+ T cells to increase their abundance during virus infection. J. Exp. Med. *201*, 1053–1059.

41. Gocher, A.M., Workman, C.J., and Vignali, D.A.A. (2022). Interferon-γ: teammate or opponent in the tumour microenvironment? Nat. Rev. Immunol. *22*, 158–172.

42. Moningi, S., Dholakia, A.S., Raman, S.P., Blackford, A., Cameron, J.L., Le, D.T., De Jesus-Acosta, A.M.C., Hacker-Prietz, A., Rosati, L.M., Assadi, R.K., et al. (2015). The Role of Stereotactic Body Radiation Therapy for Pancreatic Cancer: A Single-Institution Experience. Ann. Surg Oncol. *22*, 2352–2358.

43. Ye, J., Mills, B.N., Zhao, T., Han, B.J., Murphy, J.D., Patel, A.P., Johnston, C.J., Lord, E.M., Belt, B.A., Linehan, D.C., and Gerber, S.A. (2020). Assessing the Magnitude of Immunogenic Cell Death Following Chemotherapy and Irradiation Reveals a New Strategy to Treat Pancreatic Cancer. Cancer Immunol. Res. *8*, 94–107.

44. Mills, B.N., Qiu, H., Drage, M.G., Chen, C., Mathew, J.S., Garrett-Larsen, J., Ye, J., Uccello, T.P., Murphy, J.D., Belt, B.A., et al. (2022). Modulation of the Human Pancreatic Ductal Adenocarcinoma Immune Microenvironment by Stereotactic Body Radiotherapy. Clin. Cancer Res. *28*, 150–162.

45. Hannon, G., Lesch, M.L., and Gerber, S.A. (2023). Harnessing the Immunological Effects of Radiation to Improve Immunotherapies in Cancer. Int. J. Mol. Sci. *24*, 7359.

46. Lee, H.-G., Cho, M.-J., and Choi, J.-M. (2020). Bystander CD4+ T cells: crossroads between innate and adaptive immunity. Exp. Mol. Med. *52*, 1255–1263.

47. Mills, K.H.G. (2011). TLR-dependent T cell activation in autoimmunity. Nat. Rev. Immunol. *11*, 807–822.

48. Kaur, J., Jaruvongvanich, V., and Chandrasekhara, V. (2022). Endoscopic ultrasound-guided injectable therapy for pancreatic cancer: A systematic review. World J. Gastroenterol. *28*, 2383–2395.

49. Chung, K.M., Singh, J., Lawres, L., Dorans, K.J., Garcia, C., Burkhardt, D.B., Robbins, R., Bhutkar, A., Cardone, R., Zhao, X., et al. (2020). Endocrine-Exocrine Signaling Drives Obesity-Associated Pancreatic Ductal Adenocarcinoma. Cell *181*, 832–847.e18.

50. Zhu, Y., Knolhoff, B.L., Meyer, M.A., Nywening, T.M., West, B.L., Luo, J., Wang-Gillam, A., Goedegebuure, S.P., Linehan, D.C., and De Nardo, D.G. (2014). CSF1/CSF1R blockade reprograms tumor-infiltrating macrophages and improves response to T-cell checkpoint immunotherapy in pancreatic cancer models. Cancer Res. *74*, 5057–5069.

51. Jain, R., Frederick, J.P., Huang, E.Y., Burke, K.E., Mauger, D.M., Andrianova, E.A., Farlow, S.J., Siddiqui, S., Pimentel, J., Cheung-Ong, K., et al. (2018). MicroRNAs Enable mRNA Therapeutics to Selectively Program Cancer Cells to Self-Destruct. Nucleic Acid Ther. *28*, 285–296.

OMTN, Volume *35*

Supplemental information

Integrating IL-12 mRNA nanotechnology with SBRT eliminates T cell exhaustion in preclinical models of pancreatic cancer

Angela L. Hughson, Gary Hannon, Noah A. Salama, Tara G. Vrooman, Caroline A. Stockwell, Bradley N. Mills, Jesse Garrett-Larsen, Haoming Qiu, Roula Katerji, Lauren Benoodt, Carl J. Johnston, Joseph D. Murphy, Emma Kruger, Jian Ye, Nicholas W. Gavras, David C. Keeley, Shuyang S. Qin, Maggie L. Lesch, Jason B. Muhitch, Tanzy M.T. Love, Laura M. Calvi, Edith M. Lord, Nadia Luheshi, Jim Elyes, David C. Linehan, and Scott A. Gerber

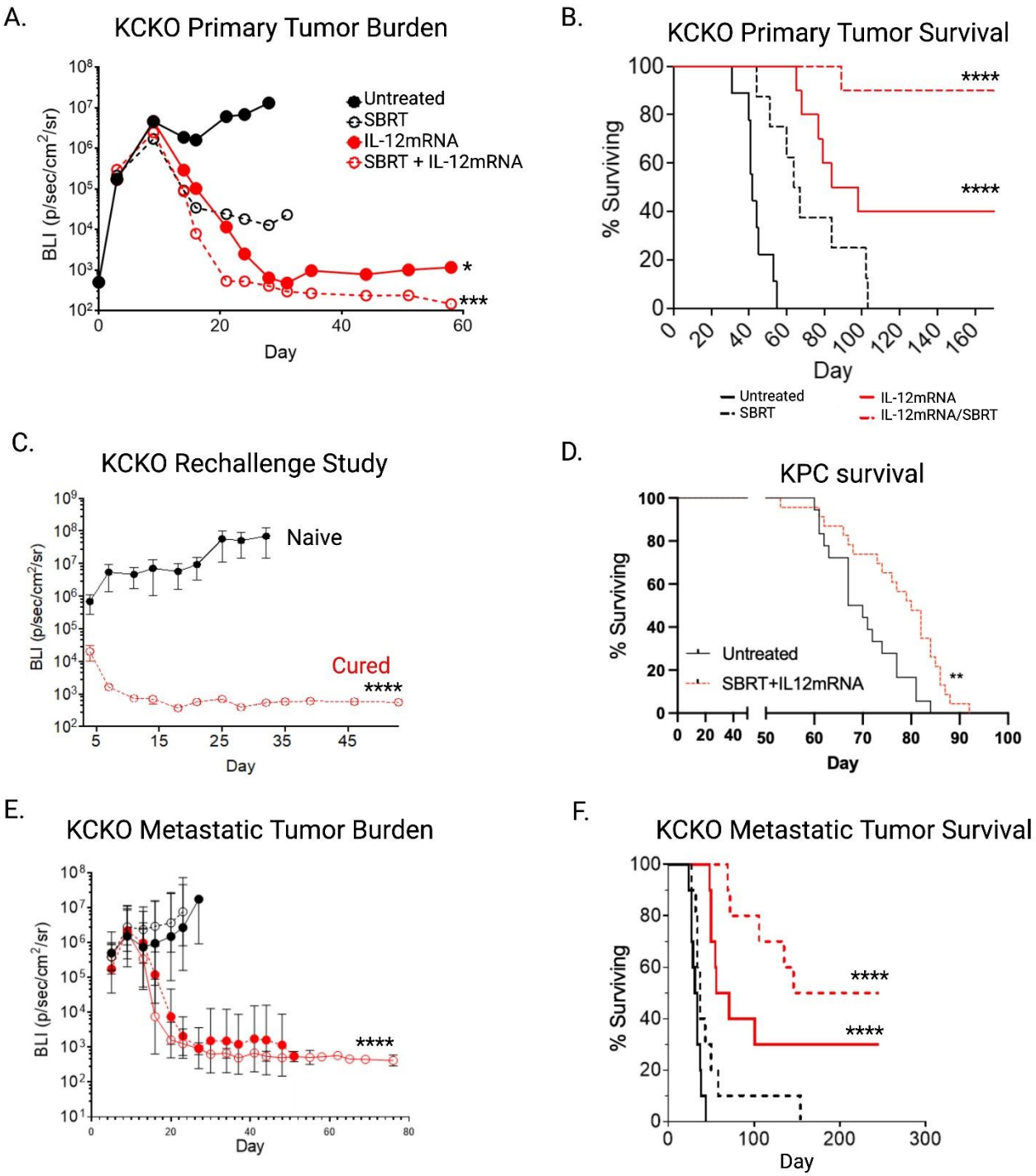

Figure S1. Combination treatment controls tumor burden and improves survival in multiple PDAC mouse models. (**A**) KCKO cells were injected orthotopically and treated with or without SBRT (6Gy/day over 4 consecutive days) followed by an intratumoral injection of IL-12mRNA or scr-mRNA 1 day after the final fraction of radiation. Tumor burden was assessed by BLI measurements. (**B**) Survival of KCKO model followed for >160 days. (**C**) Mice cured of KCKO tumors following SBRT and IL-12mRNA treatment for 150 days were rechallenged with a hemi-spleen injection of KCKO-Luc to induce hepatic metastases. Liver tumor burden was assessed by IVIS. Aged-matched naïve mice were used as controls. (**D**) KPC mice were assessed for tumor at 5 weeks of age and fiducial clips inserted accordingly. SBRT (6G/day over 4 consecutive days) followed by an intratumoral injection of IL-12mRNA or control scr-mRNA 1 day after the final fraction of radiation was administered and survival monitored. (**E**) KCKO primary tumors were implanted along with liver metastasis and primary tumors were treated with SBRT and IL-12mRNA. Tumor burden was measured by BLI. (**F**) Survival of metastatic KCKO model. n=10/group from 3 independent experiments in A & B; n=5 naïve and n=7 cured in C; n=18 for Untreated and n=23 for SBRT + IL-12mRNA in D. n=10 in E and F. *p<0.05;**p<0.01; ***p,0.001 ****p<0.0001. Error bars represent SEM in (**C**) and (**E**).

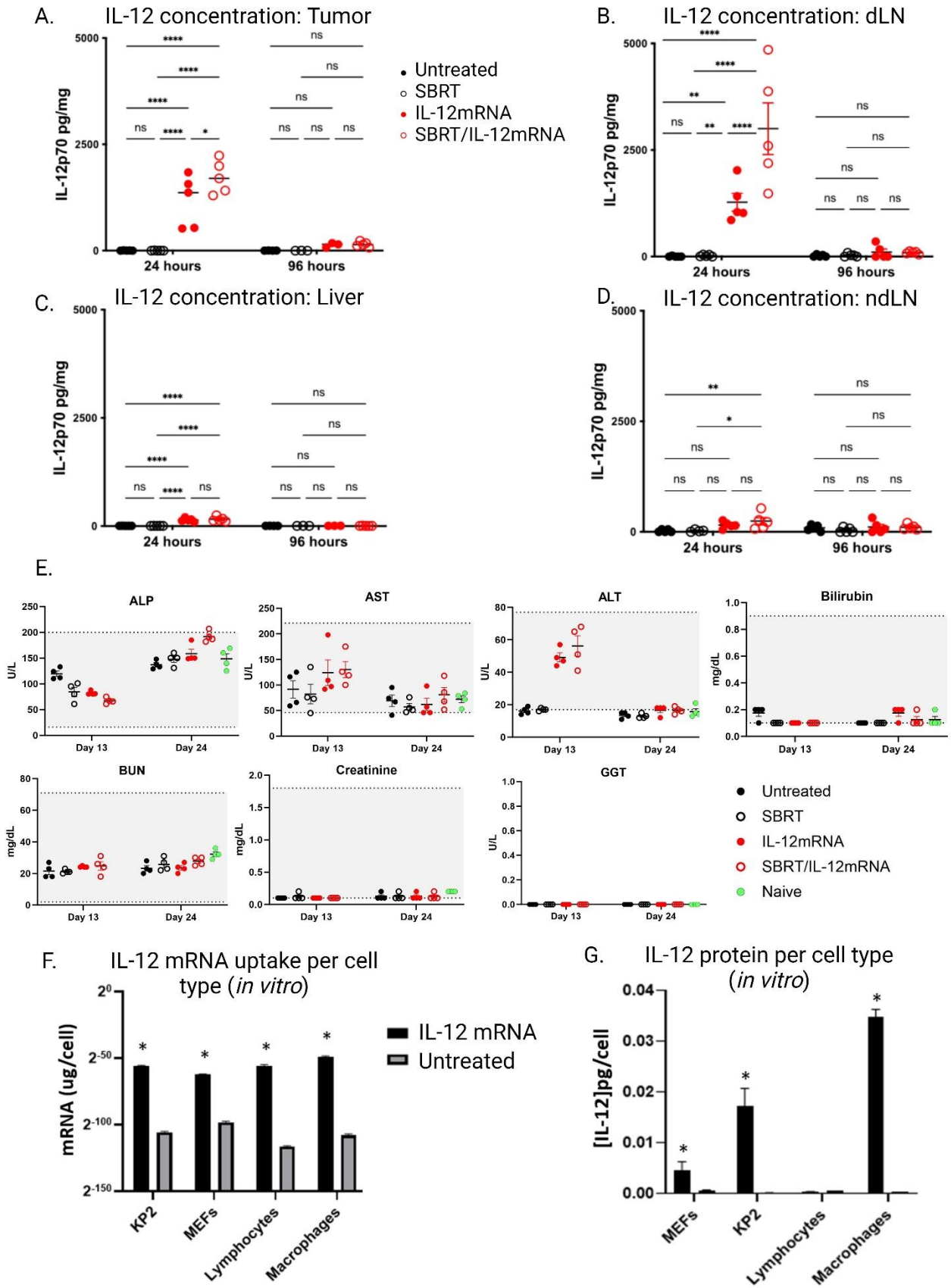

Figure S2. Assessment of IL-12 concentration following treatment. Mice were inoculated with KP2 tumor cells and treated as detailed in **Figure 1A**. 24 and 96 hours after intratumoral injection of IL-12mRNA or scr-mRNA, tissues were removed, homogenized, and assayed for IL-12p70 protein by Luminex. IL-12 concentration was determined following standardization to total protein (pg/mg) in (**A**) primary pancreatic tumors, (**B**) pancreatic tumor-draining lymph node, (**C**)

liver, and (**D**) non-draining (inguinal) lymph node. Y-axis is kept uniform to compare across tissues. (**E**) Mice were inoculated with KP2 tumors and treated as before. On days 13 and 24 post inoculation, serum was isolated from mice in each treatment group along with naïve, non-tumor bearing controls and assessed for biochemical analysis of liver (alkaline phosphatase: ALP, aspartate transaminase: AST, alanine transaminase: ALT, gamma-glutamyl treanspeptidase: GGT, and bilirubin) and kidney function (blood urea nitrogen: BUN, and creatinine). Grey regions depict normal physiological levels for each respective marker. (**F**) Cultured cells consisting of KP2, mouse embryonic fibroblasts (MEFs), naïve CD4/CD8 lymphocytes, and peritoneal lavage macrophages were treated with IL-12mRNA or scr-mRNA *in vitro* for 24 hours and assayed for a unique sequence in IL-12mRNA by qPCR (**E**) or IL-12 protein by ELISA (**G**). Values are standardized to number of total cells recovered at endpoint. n=5 mice/group in A-D; In E&F, each sample well was performed in triplicate and experiment repeated three times. Analyzed by one-way ANOVA followed by Tukey's test in A-D; student t-test in E&F comparing IL-12mRNA to scRNA in each group. *p<0.05;**p<0.01; ****p<0.0001. Lines represent mean±SEM in (**A**) – (**E**) and error bars indicate SEM in (**F**) and (**G**).

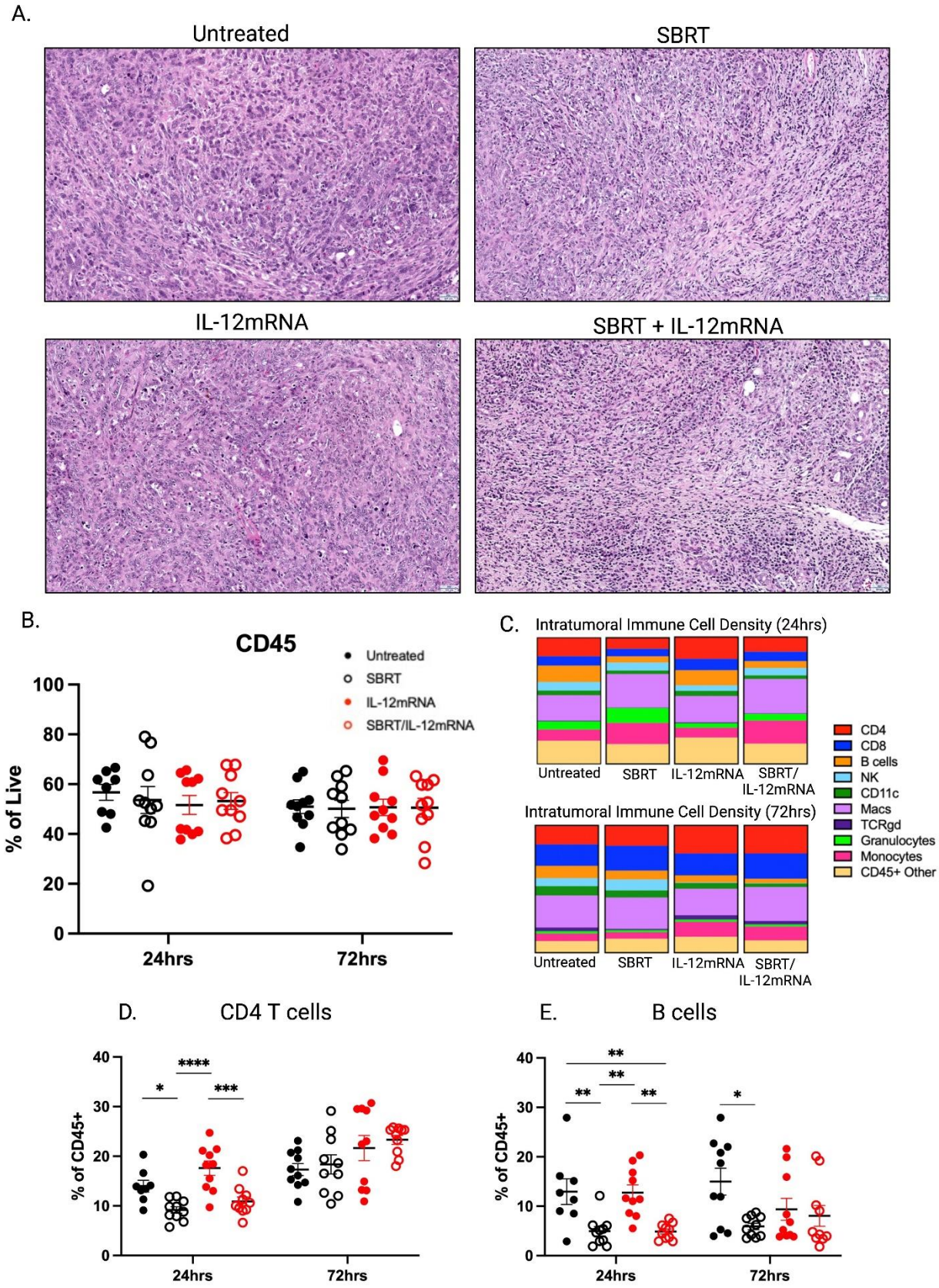

Figure S3. Effects of SBRT/IL-12mRNA on the tumor microenvironment. (**A**) Representative H&E images of tumors 72hrs post IL-12mRNA/scRNA injection (20X magnification). (**B & C**) Flow cytometry analysis of immune subsets across all treatments and time points. (**D & E**) Frequency of CD4 T cells and B cells 24hrs and 72hrs post IL-12mRNA/scr-mRNA injection for each treatment group. n=8-10 for B, D and E. Analyzed by one-way ANOVA followed by Tukey's test in C. *p<0.05; **p<0.01; ****p<0.0001. Scale bar represents 200um in A. Lines represent mean±SEM in (**B**), (**D**), and (**E**).

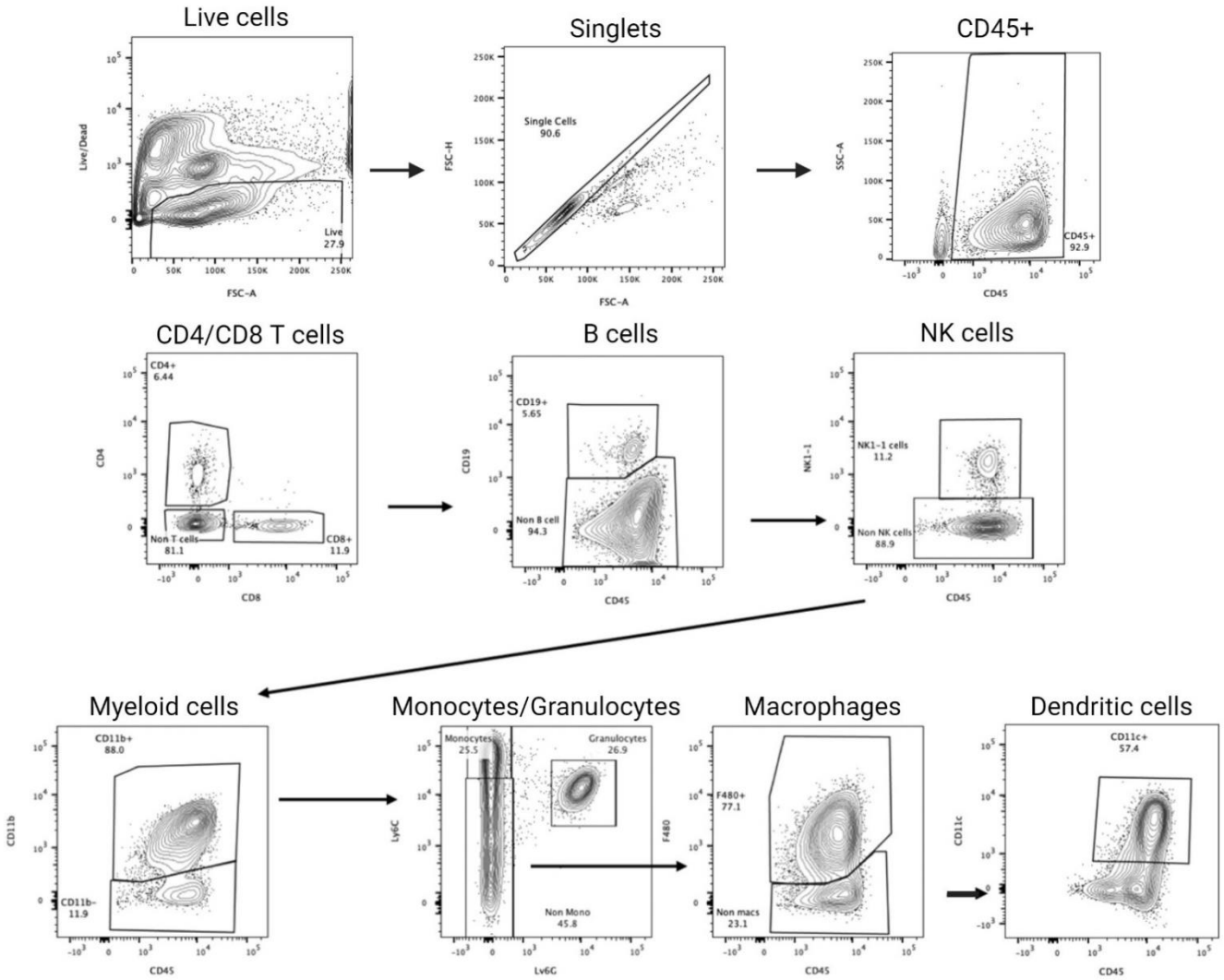

Figure S4: Gating strategy for determining immune subsets. Tumors were treated as described in **Figure 1A** and were harvested at 24 and 72 hours post IL-12 mRNA/scr-mRNA injection and stained for various markers to determine changes to immune subsets. Live cells (Ghost dye-) were gated against FSC-A and doublets were removed. CD45+ cells were gated and used to determine CD4+ and CD8+ T cells. Cells negative for CD4 and CD8 were used to gate B cells (CD19+), NK cells (NK1.1+) and myeloid cells (CD11b+). Myeloid cells were used to identify monocytes (Ly6C+), granulocytes (Ly6G+Ly6C+), macrophages (Ly6C-F480+) and dendritic cells (F480-CD11c+).

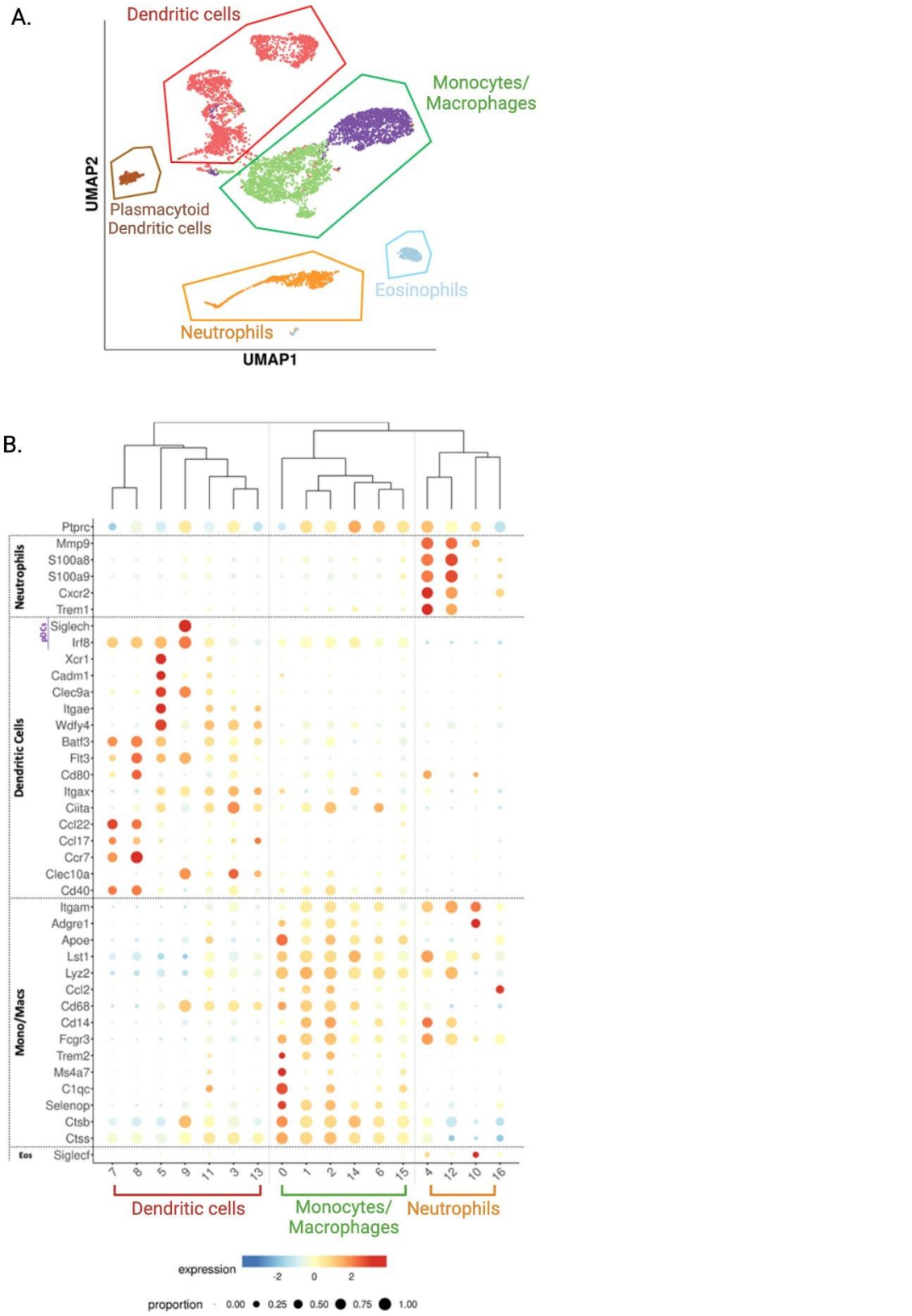

Figure S5. Identifying myeloid populations with scRNA-seq. (**A**) Combined UMAP of all myeloid cells used to identify populations of dendritic cells, monocytes/macrophages, neutrophils and eosinophils based on canonical markers. (**B**) Dot plots of canonical markers highlighting the different populations of myeloid cells.

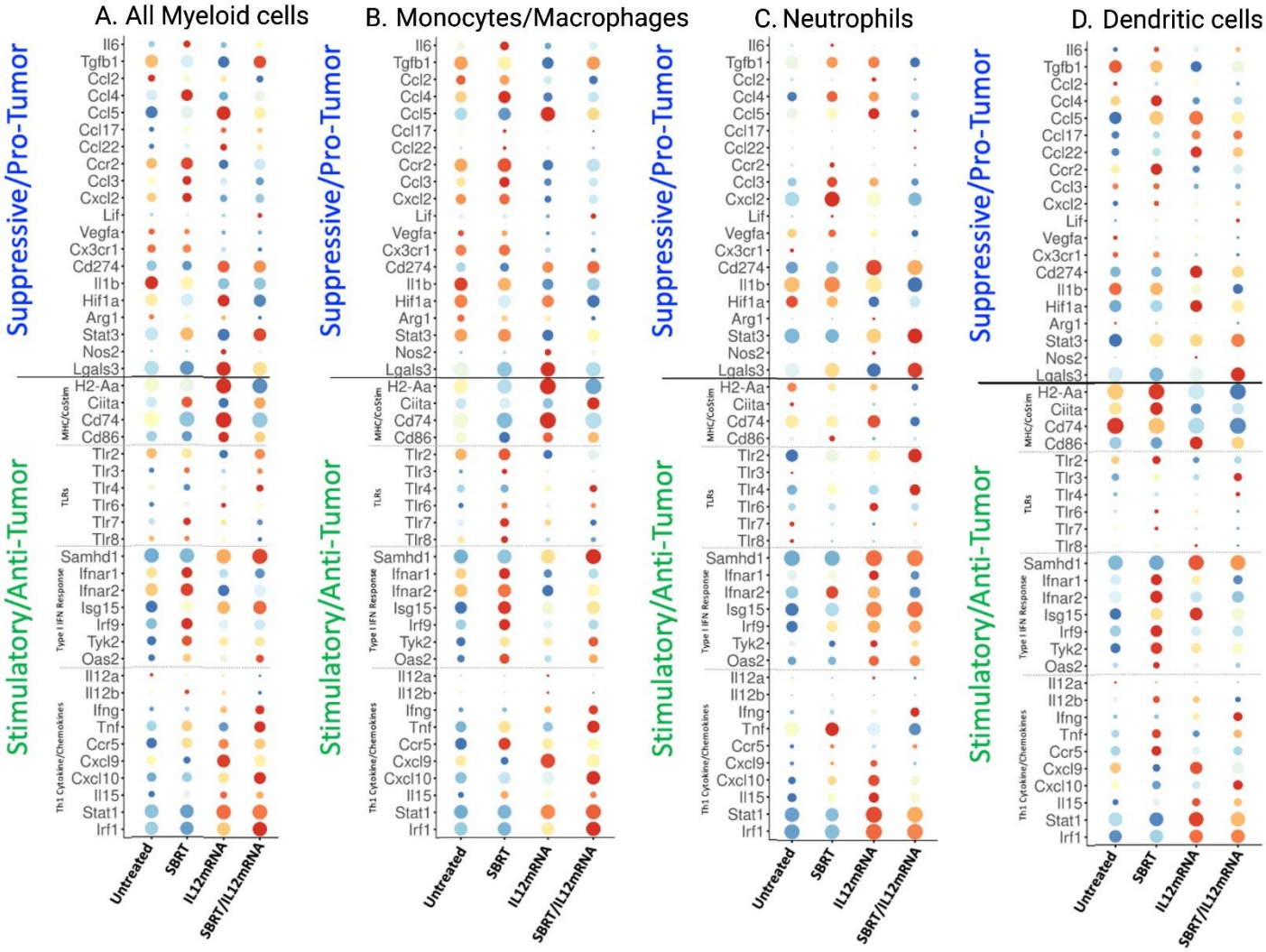

Figure S6. Expression of immunostimulatory and immunosuppressive genes in myeloid populations following treatment. Canonical immunostimulatory and immunosuppressive gene expression in (**A**) All Myeloid cells, (**B**) Monocytes and Macrophages, (**C**) Neutrophils and (**D**) Dendritic cells following treatment.

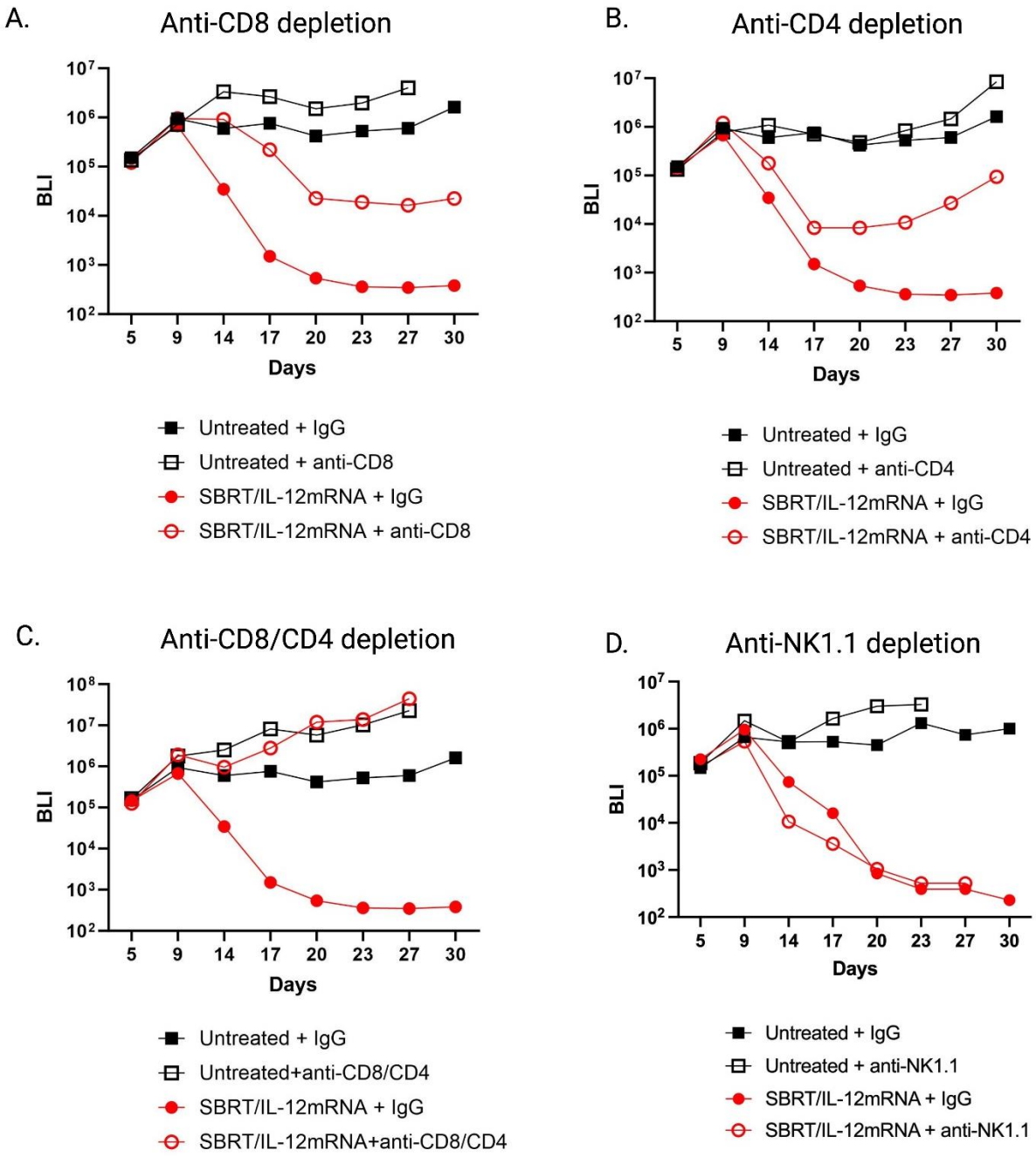

Figure S7. BLI growth curves following antibody depletion of effector cell populations during and after SBRT/IL-12mRNA treatment. (**A**) CD8 T cell depletion with isotype control for untreated and SBRT/IL-12mRNA treated mice. (**B**) CD4 T cell depletion with isotype control for untreated and SBRT/IL-12mRNA treated mice. (**C**) CD4 and CD8 T cell depletion with isotype control for untreated and SBRT/IL-12mRNA treated mice. (**D**) NK cell depletion with isotype control for untreated and SBRT/IL-12mRNA treated mice. In all cases, depletions began at Day 5 post tumor implantation (1 day prior to the first fraction of SBRT) and continued every 3 Days for a total of 7 doses. n=10 for each group.

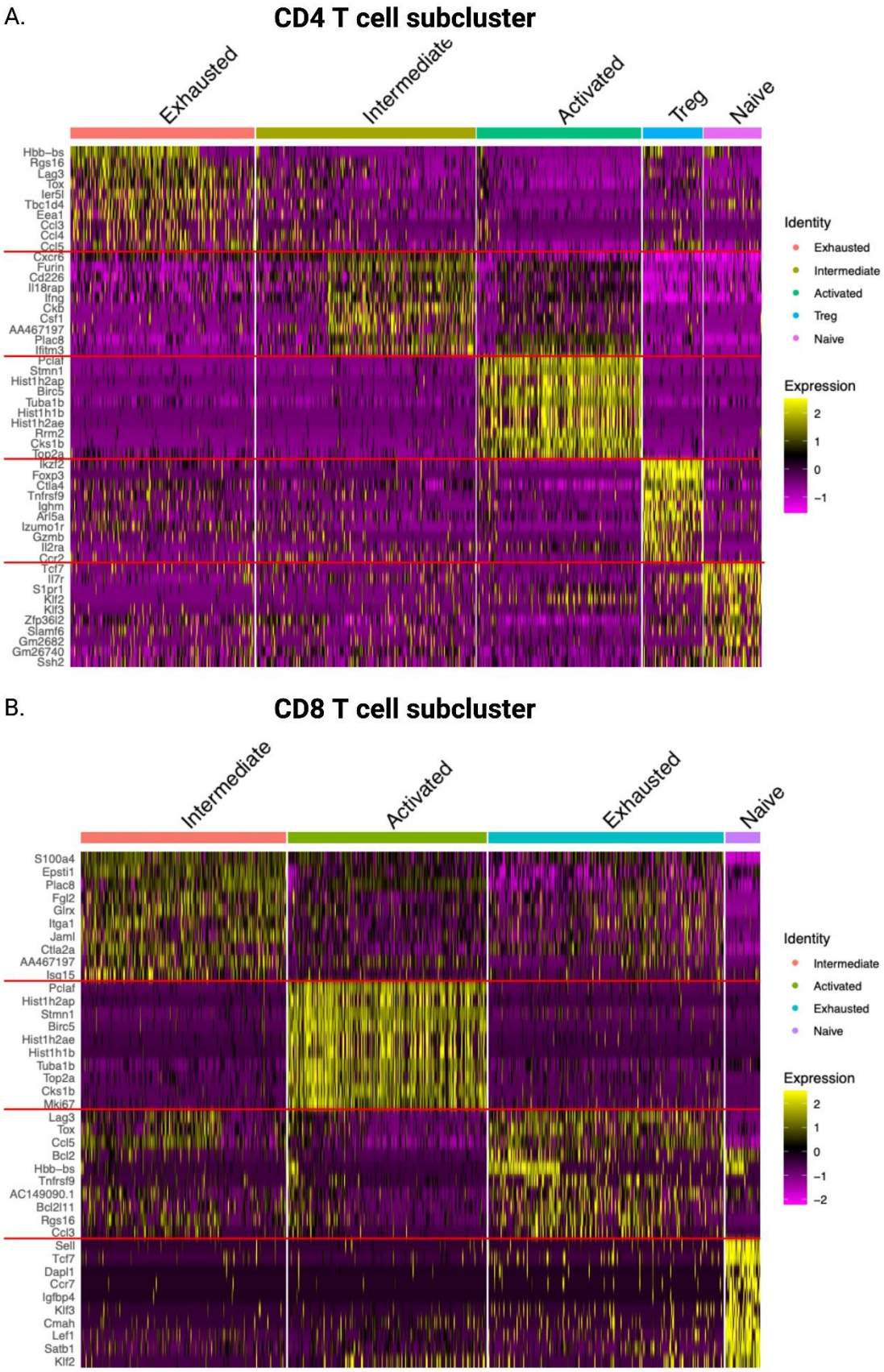

Figure S8. Differentially expressed genes for each subcluster of CD4 and CD8 T cells. Top 10 differentially expressed genes for each subcluster of CD4 (**A**) and CD8 (**B**) T cells are presented in heat maps.

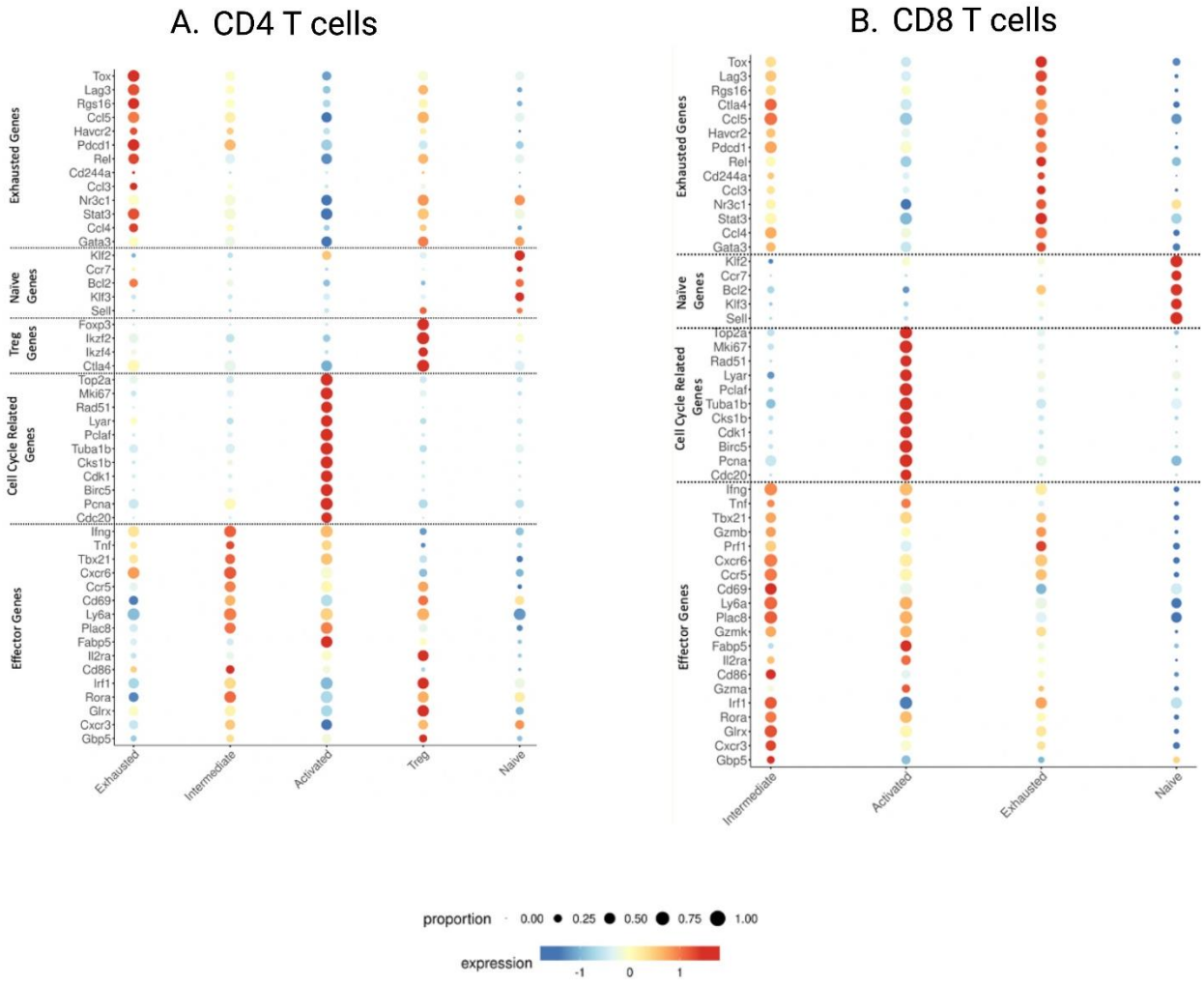

Figure S9. Classifying T cell subsets based on hallmark genes. Dot plots highlight expression levels of hallmark genes for a given proportion of cells associated with each subcluster of CD4 (**A**) and CD8 (**B**) T cells.

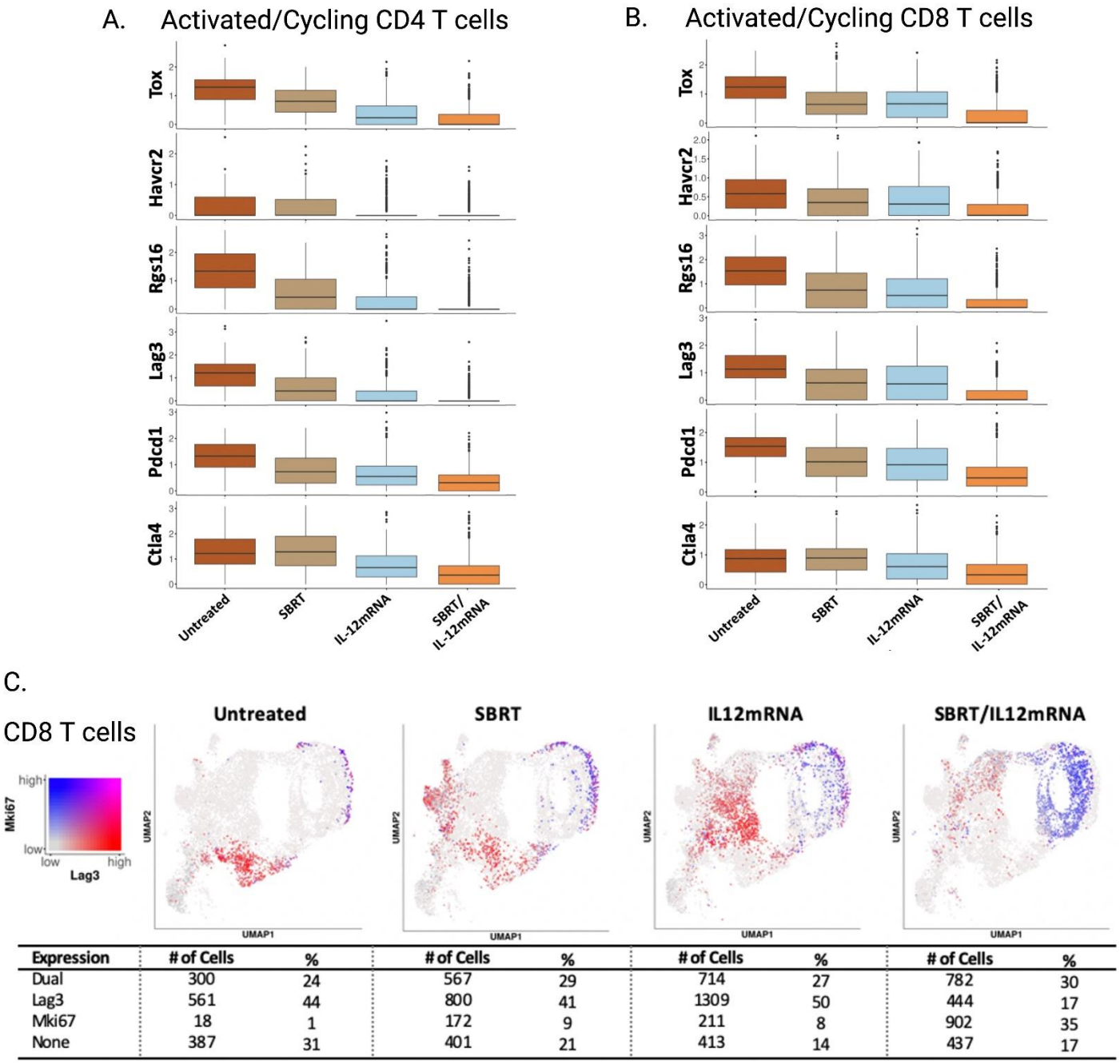

Expression	# of Cells	%	# of Cells	%	# of Cells	%	# of Cells	%
Dual	300	24	567	29	714	27	782	30
Lag3	561	44	800	41	1309	50	444	17
Mki67	18	1	172	9	211	8	902	35
None	387	31	401	21	413	14	437	17

Figure S10. Expression of key genes in CD4 and CD8 T cells post treatment. (**A & B**) Boxplot depicting exhaustion marker expression in activated/cycling CD4 and CD8 T cells following treatment. (**C**) A marked reduction in exhaustion marker Lag3 is accompanied by an upregulation of proliferative marker Mki67 after SBRT/IL-12mRNA treatment.

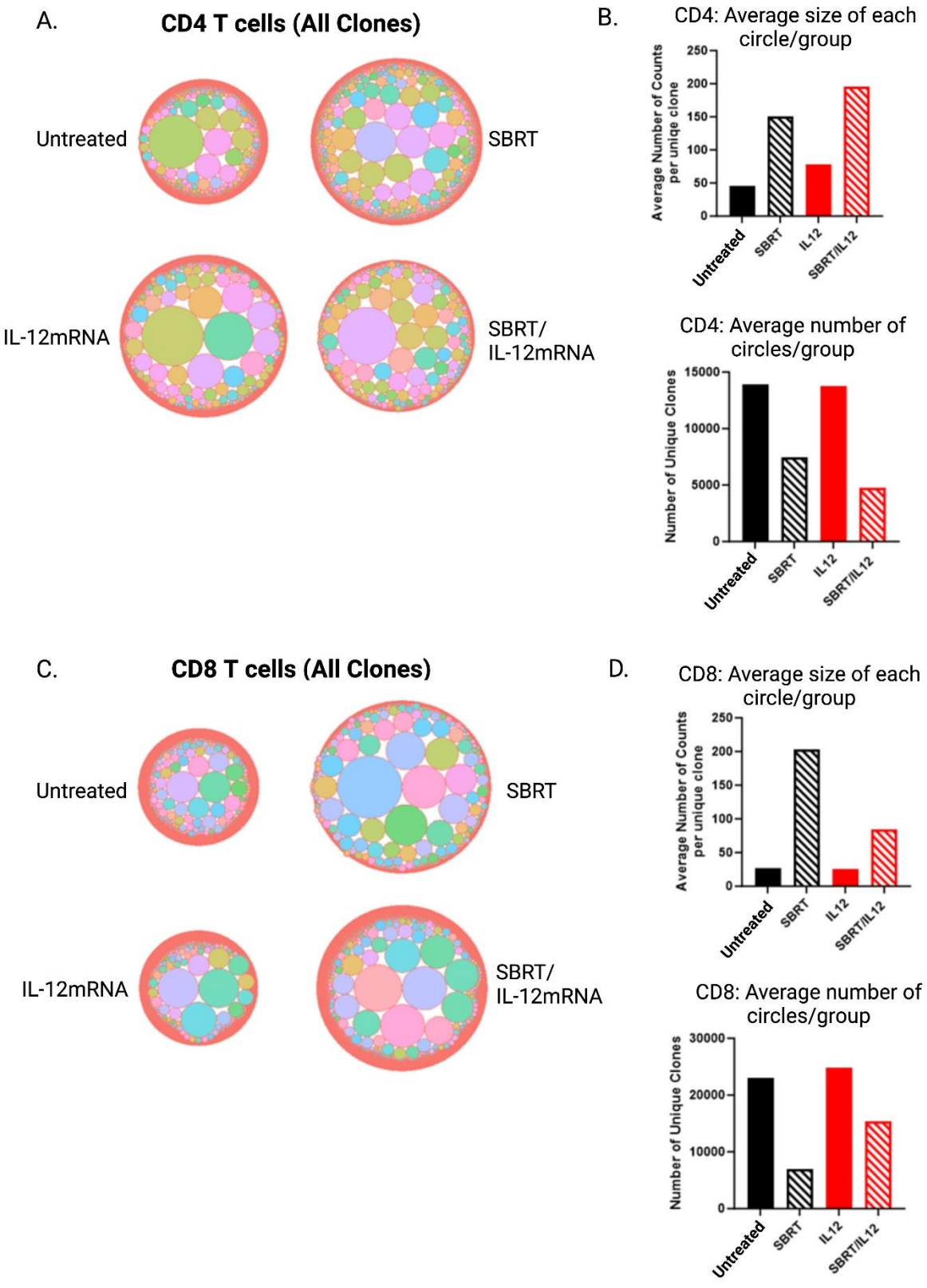

Figure S11. Downsampled population of CD4 and CD8 T cell clonotypes. Bubbleplots and accompanied bar charts depicting the downsampled size of T cell receptor clones and their relative abundance for CD4 T cells (**A & B**) and CD8 T cells (**C & D**).

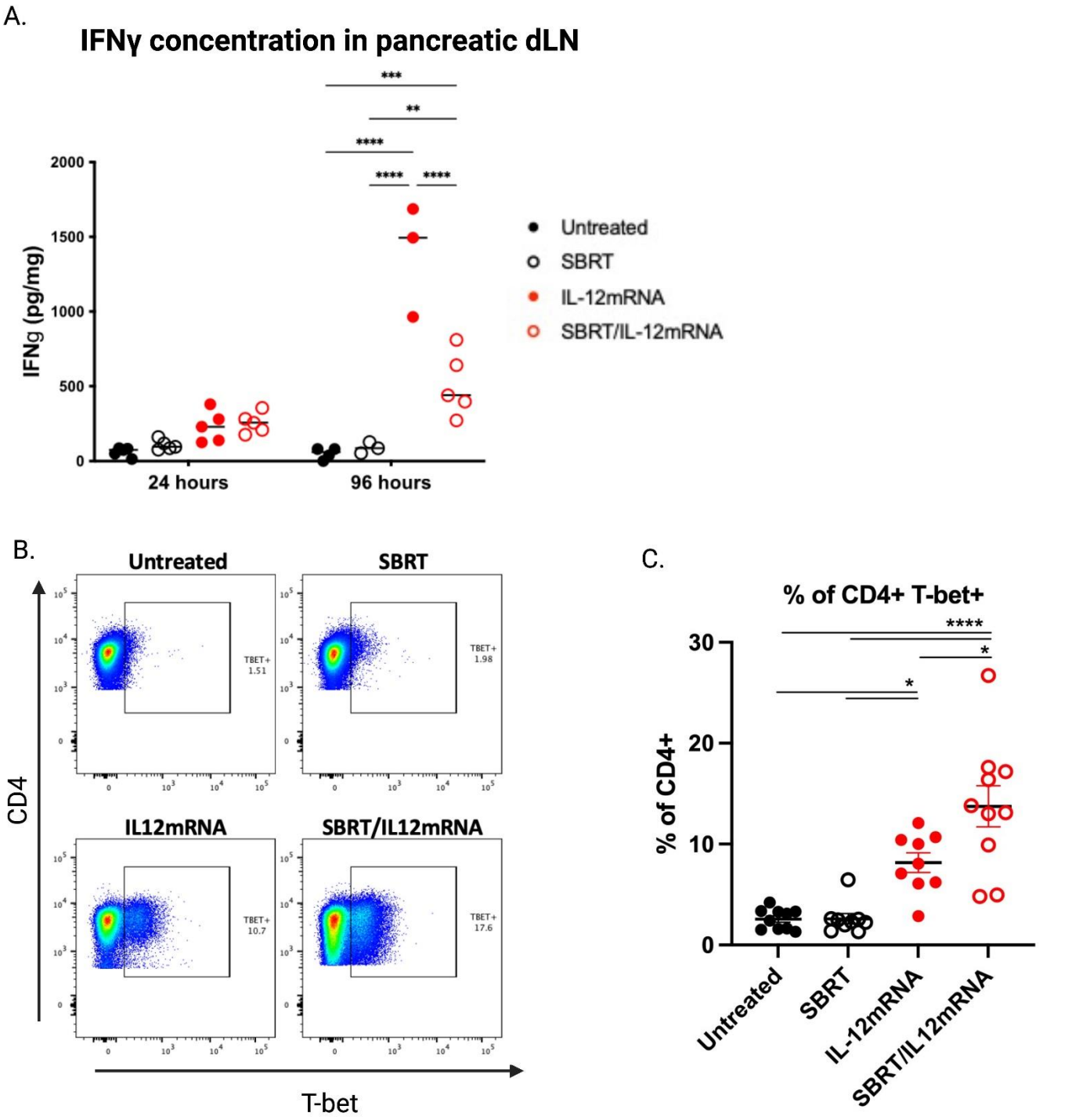

Figure S12. Quantifying IFNγ and T-bet expression in pancreatic draining lymph node following treatment. (**A**) IFNγ is significantly increased in the pancreatic draining lymph node 96 hours post IL-12mRNA/scr-mRNA injection. (**B**) Representative flow plots for T-bet staining of CD4 T cells. (**C**) Significant increases of T-bet+ CD4 T cells in the draining lymph node were were determined at 72hrs post IL-12mRNA/scr-mRNA injection. Both A and C were analyzed by one-way ANOVA and Tukey's test. Significance is compared against the untreated and within treatments. n=5 for (A); n=9-10 for (B). *p<0.5; **p<0.01; ****p<0.0001. Lines represent mean±SEM in (**C**).

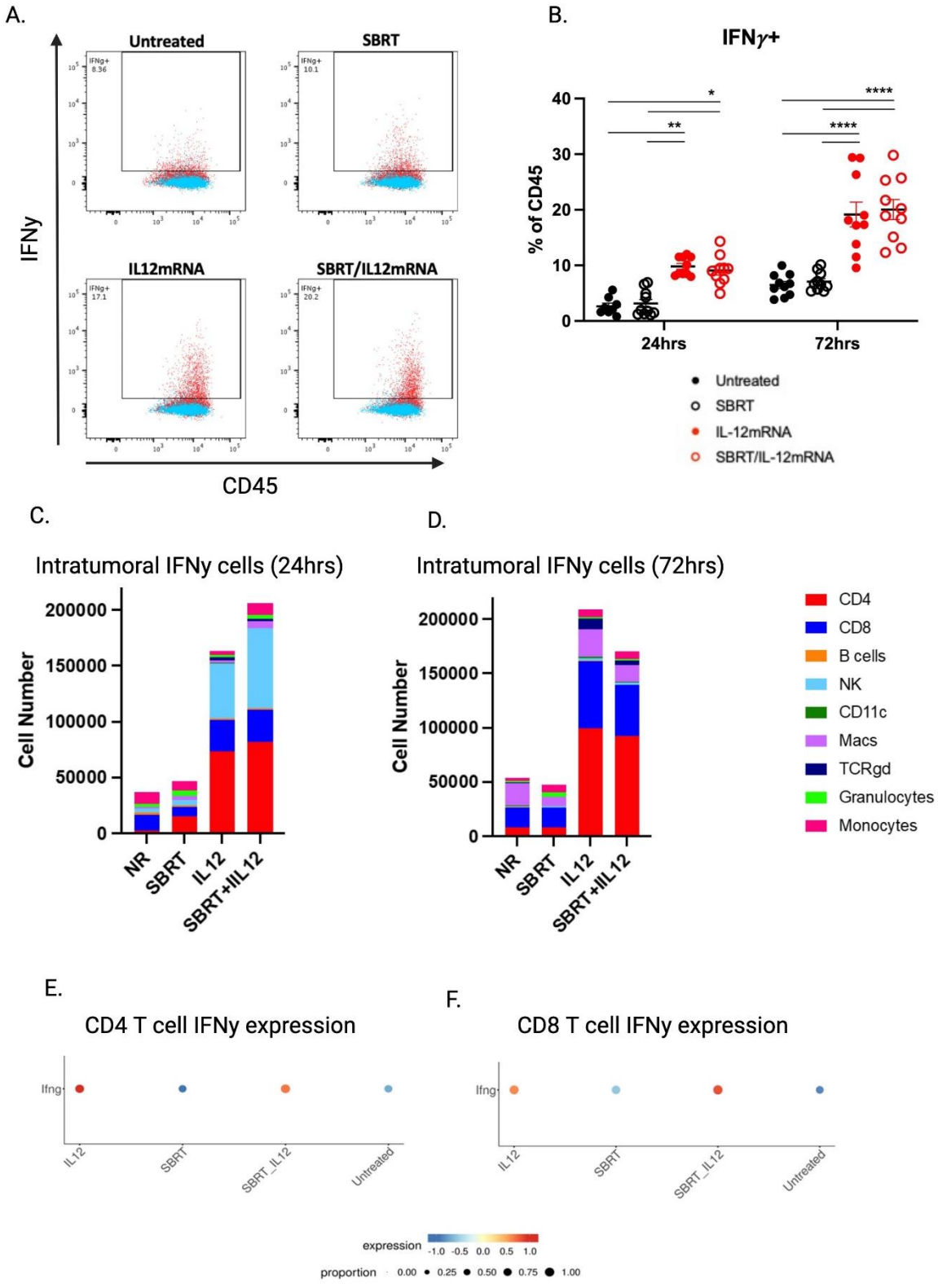

Figure S13. Expression of IFNγ in the tumor microenvironment following treatment. (**A**) Representative flow plots for IFNγ staining of CD45+ cells from the tumor microenvironment. Blue events indicate FMO control, red events correspond to IFNγ staining. (**B**) Tumor levels of IFNγ+ CD45+ cells 24hrs and 72hrs post IL-12mRNA/scr-mRNA injection. (**C & D**) Relative numbers of IFNγ+ intratumoral immune cells 24hrs and 72hrs post IL-12mRNA/scr-mRNA injection. (**E & F**) Gene expression of IFNγ+ by CD4 and CD8 T cells is mediated by IL-12mRNA. B was analyzed by one-way ANOVA followed by Tukey's test. *p<0.05; **p<0.01; ****p<0.0001. Lines represent mean±SEM in (**B**).